Global analysis of periodic orbit bifurcations in coupled Morse oscillator systems: time-reversal symmetry, permutational representations and codimension-2 collisions

Masa Tsuchiya[a),b)] and Gregory S. Ezra[c)]
Department of Chemistry and Chemical Biology, Cornell University, Ithaca, New York 14853

(Received 19 April 1999; accepted for publication 26 July 1999)

In this paper we study periodic orbit bifurcation sequences in a system of two coupled Morse oscillators. Time-reversal symmetry is exploited to determine periodic orbits by iteration of symmetry lines. The permutational representation of Tsuchiya and Jaffé is employed to analyze periodic orbit configurations on the symmetry lines. Local pruning rules are formulated, and a global analysis of possible bifurcation sequences of symmetric periodic orbits is made. Analysis of periodic orbit bifurcations on symmetry lines determines bifurcation sequences, together with periodic orbit periodicities and stabilities. The correlation between certain bifurcations is explained. The passage from an integrable limit to nonintegrability is marked by the appearance of tangent bifurcations; our global analysis reveals the origin of these ubiquitous tangencies. For period-1 orbits, tangencies appear by a simple disconnection mechanism. For higher period orbits, a different mechanism involving 2-parameter collisions of bifurcations is found. © *1999 American Institute of Physics.* [S1054-1500(99)00704-1]

Knowledge of classical periodic orbits and their bifurcations is of great importance in the study of nonintegrable Hamiltonian systems. Periodic orbits also play an essential role in investigations of the classical-quantum correspondence for such systems. In this paper, we provide a detailed study of the periodic orbits in a model Hamiltonian describing molecular vibrations. Symmetries arising from invariance of the equations of motion under time-reversal are fully exploited, as is a new permutational representation of the periodic orbits. In this way, a global understanding of possible bifurcation sequences is possible.

I. INTRODUCTION

The importance of the study of periodic orbits (pos) in nonintegrable classical Hamiltonian systems has been appreciated since the time of Poincaré.[1–3] Knowledge of po locations and stabilities provides an understanding of phase space structure and transport.[3] Quantities such as escape rates and correlation functions can be expressed in terms of po properties.[4]

Much interest attaches to the process of po creation and destruction with changes in system parameter;[5] the study of po bifurcations can provide essential insights into the route from simple (integrable) dynamics to complicated, chaotic dynamics as nonintegrability is introduced.

The study of classical pos has received added impetus from recent work in semiclassical po theory on the classical-quantum correspondence in classically nonintegrable systems.[6,7] The essential result here is the Gutzwiller trace formula,[6] which is a semiclassical expression for the oscillatory part of the density of states of a quantum system in terms of the periods, actions, stability parameters and Maslov indices of the classical pos of the corresponding classical system.[6] A large amount of work has been devoted to exploring the relation between quantum properties and classical pos.[4] For both atomic[8,9] and molecular[10] systems, it is possible to extract classical po periods and actions directly from quantum spectra. For example, Delos and coworkers have applied Hamiltonian bifurcation theory to analyze po bifurcation patterns derived from spectra of the H-atom in a magnetic field.[11]

Study of classical pos is important in the interpretation of molecular vibrational spectra.[10,12–14] The pos and their associated resonance zones[15,16] provide the means to assign highly-excited states in regimes where traditional spectroscopic methods, based on a harmonic oscillator (integrable) limit picture, fail.[17]

In this paper we study the periodic orbits of a classical nonintegrable Hamiltonian describing two coupled anharmonic (Morse) oscillators. Our system is a model for molecular effective vibrational Hamiltonians used to fit spectra,[18] and consists of a zeroth-order integrable part together with a number (up to two, here) of resonant coupling terms. The motivation for our work is the need to understand the organization of classical pos in our system, in order to be able to analyze the quantum spectrum via semiclassical po theory.[19] Special emphasis is placed on the classical po bifurcation sequences. However, the present investigation of the classical bifurcations stands alone as a systematic attempt to understand the transition from integrability to nonintegrability in a fairly typical molecular vibrational Hamiltonian.

Bifurcations of fundamental classical pos have been studied in detail by Kellman and coworkers for the integrable

a)Electronic mail: tsuchiya@stanford.edu
b)Present address: Department fo Chemistry, Stanford University, Stanford, CA 94305.
c)Electronic mail: gse1@cornell.edu

case where only a single (1:1[20] or 2:1[21]) coupling term is present. Moreover, semiclassical po theory has been applied to these integrable systems.[22,23] Although the integrable limit manifests rich structure in the dependence of phase space structure on system parameter,[20,21] it is necessary to understand what happens as integrability is broken by the presence of an additional coupling term.[24]

Efficient and systematic determination of pos in both area-preserving maps and continuous time Hamiltonian systems requires the exploitation of symmetries associated with the invariance of equations of motion under involution operations such as time-reversal.[25–27] The search for pos in the 2D surface of section is then reduced to an analysis of the intersections of the *symmetry line* with its iterates under the return map,[25,26,28] as intersection points must lie on pos.[25] A key problem then becomes one of understanding the organization of (symmetric) pos along the symmetry line.

A new approach to this problem has recently been developed by Tsuchiya and Jaffé (TJ) in their study of periodic and homoclinic bifurcations in the area-preserving Hénon map.[28] A *permutational representation* is used to describe the intersection configuration of a symmetry line and its iterate, and thereby enumerate pos and their periodicities for a given order of iteration. Using the permutational representation to understand po organization at each order of iteration enables one to construct the whole set of (symmetric) pos. Local topological constraints on the way in which orbits appear and disappear then allow the formulation of *pruning rules*, which in turn enable the *global* bifurcation structure for symmetric pos to be elucidated. This analysis is described in more detail below, while the mathematical foundation for the permutational representation is provided in Ref. 28. For the case of the area-preserving Hénon map, for which the strong coupling limit is fully chaotic (hyperbolic), it is possible to develop a full understanding of po bifurcation patterns.[28]

As described in more detail in Tsuchiya's thesis,[28] the full power of the permutational representation approach is illustrated by the ability to generate the permutational representation for *any* order of iteration of the (hyperbolic) Hénon map T from knowledge of the intersection of the symmetry line S_i with its first iterate TS_i $(i=1,2)$, using a set of indices (cf. Sec. IV C of the present paper). Once the permutation representation is determined, global bifurcation analysis follows via the pruning rules. Furthermore, TJ have also applied the permutational analysis to homoclinic orbit bifurcations on the stable and unstable manifolds of the primary unstable fixed point. (Full accounts of this work are currently in preparation.[28]) However, since the coupled Morse system considered here is a mixed system, where no indices exist, the permutational representations are obtained fully numerically for $S_i \cap T^m S_i$, $m \neq 2^n$; for $m=2^n$, the permutational representation can always be determined.

In the present paper we apply this approach to the coupled Morse Hamiltonian. We extend the theory by using winding numbers to characterize pos; this extension is helpful for formulating pruning rules for symmetric pos in continuous-time Hamiltonian systems, as opposed to area-preserving maps.[28] Several distinct pruning sequences may be possible for a given po sequence. In addition to determining these sequences, our global analysis of the coupled Morse system reveals the mechanism responsible for the appearance of ubiquitous tangent bifurcations in the nonintegrable case. Moreover, by analyzing po pairing on two symmetry lines, we can obtain information on po stabilities, hence changes in local phase space structure. Bifurcations in a coupled Morse system have also been studied by Weston and Child.[29]

This paper is organized as follows: Section II introduces the model vibrational Hamiltonian and reviews the topic of time-reversal symmetry and symmetry lines. Section III introduces the concept of the permutation representation, while Sec. IV applies the method to the integrable limit (single resonance coupling) at low and high energies. Periodic orbit pruning patterns are discussed in Sec. V, and Sec. VI examines global bifurcation patterns of symmetric pos in both the integrable and nonintegrable limits. Bifurcations occurring on the second symmetry line are discussed in Sec. VII. Conclusions are given in Sec. VIII. Some technical points are addressed in the Appendix.

This paper analysis serves as a foundation for study of the classical-quantum correspondence in our system; this work will be presented elsewhere.[19]

Our emphasis here is on a global understanding of (symmetric) po bifurcation structure; that is, we wish to understand how the results of local Hamiltonian bifurcation analysis[5] ''fit together'' in the large. In recent related work, Delos and coworkers have used normal form theory to determine the fundamental dynamical origin of certain correlations between different po bifurcations that had been noted numerically.[30] Such correlations are also the subject of the present global analysis using the permutation representation. One key finding of our work here is the importance of certain codimension-2 bifurcations in mediating the transition from integrability to nonintegrability.[31] The influence of codimension-2 bifurcations in semiclassical approximations to the density of states has recently been examined by Schomerus.[32]

II. CLASSICAL MECHANICS: SYMMETRY AND PERIODIC ORBITS

A. Classical Hamiltonian

The model vibrational Hamiltonian we study describes two anharmonic (Morse) oscillators coupled by two resonant terms, a 1:1 resonant term $\mathcal{H}^{1:1}$ and a 1:2 resonant term $\mathcal{H}^{1:2}$. In terms of canonical action-angle variables $(I_1, I_2, \theta_1, \theta_2)$, the Hamiltonian is

$$\mathcal{H}=\mathcal{H}_0+\mathcal{H}^{1:1}+\mathcal{H}^{1:2}, \tag{1}$$

where $\mathcal{H}_0$ is the zeroth-order uncoupled Morse Hamiltonian

$$\mathcal{H}_0=\omega_1 I_1+\omega_2 I_2-\alpha_1 I_1^2-\alpha_2 I_2^2, \tag{2}$$

and the resonant interaction terms are

$$\mathcal{H}^{1:1}=2\beta_{11}\sqrt{I_1 I_2}\cos(\theta_1-\theta_2), \tag{3a}$$

$$\mathcal{H}^{1:2}=2\beta_{12}\sqrt{I_1} I_2\cos(\theta_1-2\theta_2), \tag{3b}$$

and $-\pi \leqslant (\theta_1, \theta_2) \leqslant \pi$. We shall take $\omega_1 = 1.0$, $\omega_2 = 0.8$, $\alpha_1 = 0.03$ and $\alpha_2 = 0.02$.

The classical phase space structure of $\mathcal{H}$ depends on the values of the parameters E, β_{11} and β_{12}. For $\beta_{12} = 0$, the Hamiltonian $\mathcal{H}$ is integrable, and periodic orbit (po) bifurcations and classical phase space structure have been extensively studied in this limit.[20] In the present work, we focus attention on the onset of nonintegrability (chaos) as the two parameters E and β_{12} change.

Semiclassical analysis of the level spectrum of the quantum version of Hamiltonian (1) results in plots of po period τ[22] or action S[19] versus energy E. Interpretation of these results therefore requires investigation of families of classical pos and their bifurcations in the classical system (1) as a function of the two parameters E and β_{12}.

B. Time reversal symmetry and symmetry lines

Our study of po bifurcations requires a systematic approach to the location of pos, as opposed to a random search in the surface of section. It is well known that periodic orbits in both area-preserving maps[25] and continuous time systems[26] can be found efficiently by locating the intersections of symmetry lines and their iterates. The symmetry lines are sets of points invariant under involution operations.[25] An important example of an involution is the operation of time reversal.

For a Hamiltonian of the usual kinetic energy plus potential form,

$$\mathcal{H} = \frac{\mathbf{p}^2}{2} + V(\mathbf{q}), \tag{4}$$

Hamilton's equations of motion $(\dot{\mathbf{q}}, \dot{\mathbf{p}}) = (\partial\mathcal{H}/\partial\mathbf{p}, -\partial\mathcal{H}/\partial\mathbf{q})$ are invariant under the time reversal operation

$$t \rightarrow -t, \tag{5a}$$

$$\mathbf{p} \rightarrow -\mathbf{p}, \tag{5b}$$

$$\mathbf{q} \rightarrow \mathbf{q}. \tag{5c}$$

The surface $\mathcal{M} = \{(\mathbf{p}, \mathbf{q}) | \mathbf{p} = \mathbf{0}, \dot{\mathbf{q}} = \mathbf{0}\}$ is therefore a ''mirror plane'': orbits initiated in this plane will follow the same trajectory in $\mathbf{q}$-space in both forward and backwards time. An orbit that returns to $\mathcal{M}$ after starting on $\mathcal{M}$ is therefore periodic. Such pos intersect $\mathcal{M}$ at two different points; it is not possible to have three or more distinct intersection points.

The model Hamiltonian (1) does not have the ''kinetic plus potential'' form. The equations of motion $(\dot{\mathbf{I}}, \dot{\boldsymbol{\theta}}) = (\partial\mathcal{H}/\partial\boldsymbol{\theta}, \partial\mathcal{H}/\partial\mathbf{I})$ are nevertheless invariant under the following time-reversal operation:

$$\theta_j(-t) = -\theta_j(t) \quad \text{or} \quad -\theta_j(t) \pm 2\pi, \quad j = 1,2 \tag{6a}$$

$$\mathbf{I}(-t) = \mathbf{I}(t), \tag{6b}$$

where the vector $(\boldsymbol{\theta}, \mathbf{I}) = (\theta_1, \theta_2, I_1, I_2)$. The mirror plane $\mathcal{M}$ is then the surface

$$\mathcal{M} = \{(\boldsymbol{\theta}, \mathbf{I}) | \theta_j = 0 \quad \text{or} \quad \pm\pi, \dot{I}_j = 0, \ j = 1,2\}, \tag{7}$$

where $\theta_j = \pi$ is identified with $\theta_j = -\pi$.

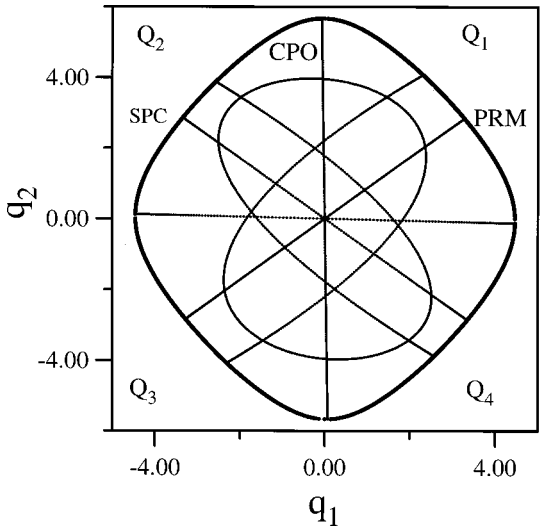

FIG. 1. Mirror boundary in (q_1, q_2) space. Points on the boundary lie at the intersection of the mirror plane $\mathcal{M}$ with the surface of constant energy, E. Four quadrants Q_i are shown, together with several important periodic orbits. Trajectories started on $\mathcal{M}$ trace out the same path in $\mathbf{q}$-space in both forward and reverse time. Energy $E = 6.98$, $\beta_{12} = 0.0$, $\beta_{11} = 0.01$.

For our model vibrational Hamiltonian (1), the intersection of the mirror plane $\mathcal{M}$ with the surface of constant energy E is topologically a circle. The four combinations of angles (θ_1, θ_2), $Q_1 \equiv (0,0)$, $Q_2 \equiv (\pi, 0)$, $Q_3 \equiv (\pi, \pi)$, and $Q_4 \equiv (0, \pi)$, are then associated with the first, second, third, and fourth quadrants of the symmetry line, respectively.

Both to facilitate numerical integration of the equations of motion and to avoid dealing with discontinuities in angular coordinates $\boldsymbol{\theta}$, we define cartesian-like coordinates $\mathbf{q}$ and conjugate momenta $\mathbf{p}$ via the canonical transformation $(I_i, \theta_i) \rightarrow (p_i, q_i)$, $i = 1,2$:

$$q_i = \sqrt{2I_i/\omega_i} \cos\theta_i, \tag{8a}$$

$$p_i = \sqrt{2I_i\omega_i} \sin\theta_i. \tag{8b}$$

From Eq. (6), we see that the time reversal operation in $(\mathbf{p}, \mathbf{q})$ space is precisely that given in Eq. (5), where on the mirror plane $\mathcal{M}$, $\mathbf{p}(t=0) = \mathbf{0}$ *and* $\dot{\mathbf{q}}(t=0) = \mathbf{0}$. At fixed energy E, the analogue of the equipotential boundary is determined by the equation

$$\mathcal{H}(\mathbf{q}, \mathbf{p} = \mathbf{0}) = E. \tag{9}$$

The mirror boundary for $E = 6.98$ is projected into $\mathbf{q}$-space in Fig. 1.

The set of trajectories initiated on the circle defined by Eq. (9) will eventually intersect the Poincaré surface of section (sos). With an appropriate choice of sectioning condition, the resulting symmetry line has a simple functional form on the sos. We define four sos by the following conditions:

$$\Sigma_1 \equiv \{\theta_2 = 0, \dot{\theta}_2 \geqslant 0\}, \tag{10a}$$

$$\Sigma_2 \equiv \{\theta_2 = \pi, \dot{\theta}_2 \geqslant 0\}, \tag{10b}$$

$$\Sigma_3 \equiv \{\theta_1 = 0, \dot{\theta}_1 \geqslant 0\}, \tag{10c}$$

TABLE I. Surfaces of section, symmetry lines and quadrants.

Section	Symmetry line	Quadrant
Σ_1	$\begin{cases} S_1 \equiv p_1 = 0 \\ S_2 = \text{image of } S_2' \end{cases}$	$\begin{cases} Q_1 \cup Q_2 \\ Q_3 \cup Q_4 \end{cases}$
Σ_2	$\begin{cases} S_2' \equiv p_1 = 0 \\ S_1' = \text{image of } S_1 \end{cases}$	$\begin{cases} Q_3 \cup Q_4 \\ Q_1 \cup Q_2 \end{cases}$
Σ_3	$\begin{cases} S_3 \equiv p_2 = 0 \\ S_4 = \text{image of } S_4' \end{cases}$	$\begin{cases} Q_1 \cup Q_4 \\ Q_2 \cup Q_3 \end{cases}$
Σ_4	$\begin{cases} S_4' = p_2 = 0 \\ S_3' = \text{image of } S_3 \end{cases}$	$\begin{cases} Q_2 \cup Q_3 \\ Q_1 \cup Q_4 \end{cases}$

$$\Sigma_4 \equiv \{\theta_1 = \pi, \dot{\theta}_1 \geqslant 0\}. \tag{10d}$$

The relation between symmetry lines S, sos Σ and quadrants Q is shown in Table I. For example, the symmetry line S_1 on sos Σ_1 is the line $p_1 = 0$. The two branches $\theta_1 = 0$ and $\theta_1 = \pi$ correspond to the union of the first and second quadrants, $Q_1 \cup Q_2$. The symmetry line S_2' on Σ_2 is the line $p_1 = 0$, and corresponds to $Q_3 \cup Q_4$. The second symmetry line S_2 on Σ_1 is the image of the set S_2'; it is not a straight line on the sos Σ_1, but has a more complicated form (see Fig. 2). The symmetry of pos that lie on S_2 in Σ_1 is therefore not as obvious as that for symmetric pos on S_1, where the relevant symmetry operation is: $p_1 \to -p_1$ and $q_1 \to q_1$. This complication for S_2 stems from the fact that the origin of time ($t = 0$) for S_2 is on the sos Σ_3, not Σ_1.

In addition to periodic orbits of finite period that start and end on symmetry lines, there can also exist symmetric homoclinic orbits, biasymptotic to the same (unstable) pos as $t \to \pm\infty$. The existence of these homoclinic orbits on the symmetry lines suggests accumulation of pos to the homoclinic orbits.[28]

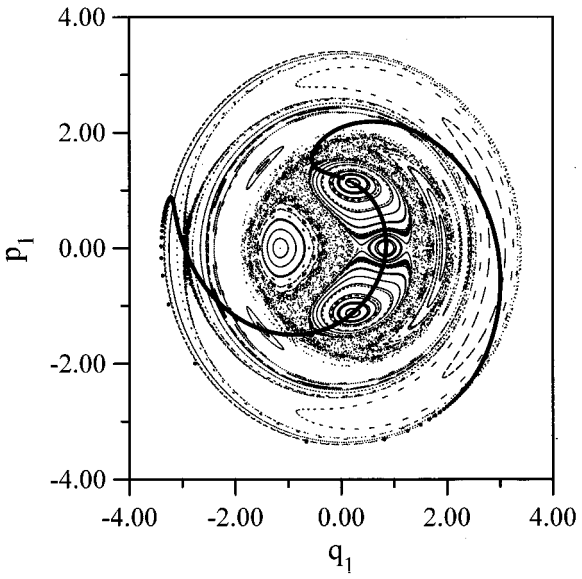

FIG. 2. Symmetry lines on the surface of section Σ_1, where Σ_1 is defined by the condition $\Sigma_1 \equiv \{\theta_2 = 0,\ \dot{\theta}_2 \geqslant 0\}$. Symmetry line S_1 is the line $p_1 = 0$, and is invariant under the momentum reversal operation $I_1 = \mathcal{R}: p_i \to -p_i$. Symmetry line S_2 is the heavy curve passing through period-1 fixed points on S_1, and is the set of points invariant under the involution $I_2 = T\mathcal{R}$. Energy $E = 4.6$, $\beta_{11} = 0.01$, $\beta_{12} = 0.02$.

In the rest of the paper, we investigate pos and their bifurcations on the Σ_1 and Σ_2 sos as the two parameters E and β_{12} vary. To study the classical-quantum correspondence, it is necessary to obtain po periods or actions as a function of energy E. Tangency problems can however arise, where, as a parameter (e.g., E) is changed, a po on Σ_1 (say) becomes tangent to Σ_1, and so disappears from the sos as the energy continues to change. In principle, such tangency problems can be eliminated by using sos defined dynamically by fundamental pos (cf. Sec. VI B 1). Missing pos also occur on the boundary of Σ_1 where $|q_1|$ has its maximum value in (p_1, q_1) space; switching to a complementary section such as Σ_3, which is still intersected by the po, the action of such orbits can still be obtained.

C. Poincaré return map as a product of involution operators

In this subsection, we summarize results on symmetric pos of area-preserving mappings that are products of two involution operators.[25–28] These results are used in setting up the permutational representation (see below).

For a continuous-time Hamiltonian system with time-reversal symmetry, such as the coupled Morse system considered in this paper, Greene showed that the Poincaré return map T, $T: \Sigma \mapsto \Sigma$, can in general be written as the product of two *involutions*:[26]

$$T = I_2 I_1, \text{ with } I_i^2 = 1 \quad (i = 1,2). \tag{11}$$

The map T is invertible, $T^{-1} = I_1 I_2$. Two symmetry lines S_i are defined as invariant sets for each involution I_i on Σ

$$S_i \equiv \{\mathbf{z} | I_i \mathbf{z} = \mathbf{z}, \mathbf{z} \in R^2\} \quad (i = 1,2). \tag{12}$$

For the coupled Morse system, one possible factorization is $I_1 = \mathcal{R}$, $I_2 = T\mathcal{R}$, where $\mathcal{R}$ is the momentum reversal operator $\mathcal{R}: p_i \to -p_i$. It is straightforward to check that $T\mathcal{R}$ is an involution, i.e., that $\mathcal{R}T\mathcal{R} = T^{-1}$, and that the symmetry line S_2 on the sos Σ_1 is invariant under I_2. The symmetry line S_1 on Σ_1 is clearly invariant under $\mathcal{R}$.

The following results can be proved:[25–28]

(1) Intersections between a symmetry line and its iterates are pos. The set of points $S_i \cap T^{n-m} S_i$ is equivalent under the mapping T^m to $T^m S_i \cap T^n S_i$.
(2) The maximum period of pos is $2n$ for intersections between the symmetry line S_i and its nth iterate $T^n S_i$, so that the po set for $S_i \cap T^n S_i$ consists of pos with periodicities that are factors of $2n$.
(3) See, e.g., Ref. 28:
   (a) If a fixed point $\mathbf{z}^{(0)}$ of a period-$2n$ periodic orbit lies on the symmetry line $S_1(S_2)$, then the n^{th} iterate of the fixed point, $\mathbf{z}^{(n)}$ also lies on the $S_1(S_2)$ symmetry line.
   (b) If a fixed point $\mathbf{z}^{(0)}$ of a period-$(2n+1)$ po lies on the $S_1(S_2)$ symmetry line, then the $(n+1)^{th}$ iterate of the fixed point $\mathbf{z}^{(n+1)}$ lies on $S_2(S_1)$.

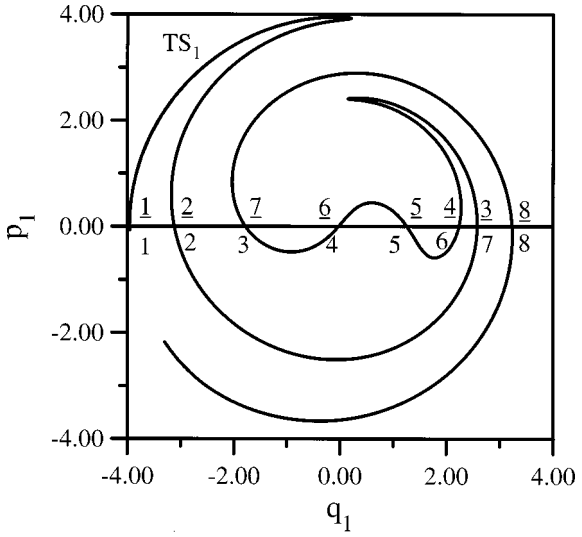

FIG. 3. Intersection of the symmetry line S_1 and its iterate TS_1 on the surface of section Σ_1. ($E=6.0$, $\beta_{12}=0.02$). The eight intersection points in $S_1 \cap TS_1$ lie on pos of period 1 or 2; the permutation $P(S_1 \cap TS_1)$ (Eq. 13) describes the configuration of fixed points.

(c) If none of the fixed points of a period-n po lies on either symmetry line, then there exists a second period-n po that is an image of the first orbit under either involution operation.
(d) No other cases occur.

III. PERMUTATIONAL REPRESENTATION OF POS

Periodic orbits are obtained by iteration of the symmetry lines. The difficulty with this (and other approaches) is that the number of symmetric pos of given period is *a priori* unknown. In this paper, we apply the method of Tsuchiya and Jaffé (TJ)[28] to both enumerate and predict the order of pos on time-reversal symmetry lines. The result of this analysis can then be used to provide a global understanding of po bifurcations.

The key idea of the TJ analysis is that a labeling of the intersections of the symmetry line and its iterate (see Fig. 3) is equivalent to a permutation. For the surface of section shown in Fig. 3, for example, the permutation $P(S_1 \cap TS_1)$ is

$$P(S_1 \cap TS_1) = \begin{pmatrix} 1 & 2 & 7 & 6 & 5 & 4 & 3 & 8 \\ 1 & 2 & 3 & 4 & 5 & 6 & 7 & 8 \end{pmatrix}. \tag{13}$$

Note that relabelling of points gives rise to a permutation that is the conjugate of the original; nevertheless, the underlying po sequence is invariant. In the usual column representation of the permutation, each column is an intersection, and hence corresponds to a point on a po. From Theorem 1 of Sec. II C, it follows that (for T a diffeomorphism), the permutational representation $P(S_i \cap T^{n-m} S_i)$ is invariant under the map T:

$$\begin{aligned} P(T^m(S_i \cap T^{n-m} S_i)) &= P(T^m S_i \cap T^n S_i) \\ &= P(S_i \cap T^{n-m} S_i). \end{aligned} \tag{14}$$

This means that study of the intersections of S_i with its iterates $T^n S_i$, $n \geqslant 1$, provides complete information on symmetric pos.

A. Structure of permutations and associated periodicities

From Theorem 3 in Sec. II C, permutations representing intersections of iterated symmetry lines consist solely of cycles of length one (unit column) $\binom{i}{i}$ or two (pair of columns) $\binom{j}{k}\binom{k}{j}$ (cf. Ref. 28). This result is easily understood by considering the time-reversal mirror $\mathcal{M}$. Orbits starting from $\mathcal{M}$ in, say, $Q_1 \cup Q_2$, either return directly to the original point after one period, or intersect $\mathcal{M}$ at a different point in $Q_1 \cup Q_2$ before returning to the original point (cf. Fig. 1), so that there are either one (unit column) or two intersection points (pair of columns) on the corresponding S_1 symmetry line. Periodicities of pos associated with $P(S_i \cap T^n S_i)$ are determined by the requirement that

$$T^n \begin{pmatrix} i \\ i \end{pmatrix} = \begin{pmatrix} i \\ i \end{pmatrix} \tag{15}$$

and

$$T^{2n} \begin{pmatrix} j \\ k \end{pmatrix} = T^n \begin{pmatrix} k \\ j \end{pmatrix} = \begin{pmatrix} j \\ k \end{pmatrix}, \tag{16}$$

so that the period corresponding to the unit column is one of the factors of n, whereas the period of the po associated with a pair of columns is a factor of $2n$, other than n itself or 1. For instance, periodicities of pos for the permutation (13) are

$$\wp(P(S_1 \cap TS_1)) = (1_1, 1_2, 2_1, 2_2, 1_3, 2_2, 2_1, 1_4), \tag{17}$$

where m_ℓ denotes the ℓ-th distinct po of period m on the sos considered. Note that, if a period-2 po appears on $S_i \cap TS_i$ as a pair of columns, then it will be represented by a unit column in $P(S_i \cap T^2 S_i)$; pos for $S_i \cap TS_i$ form a subset of the pos for $S_i \cap T^2 S_i$.

B. Generating higher order permutations from $P(S_i \cap TS_i)$: mixed systems

In order to enumerate symmetric pos, it is important to know how each order of permutation is generated from $P(S_i \cap TS_i)$ and to understand how each order of iteration organizes pos on the symmetry lines. For example, knowledge of the permutational representation for $S_i \cap T^6 S_i$ determines the relative ordering of period-3 and 4 pos on the symmetry line, which cannot be determined by knowledge of the intersections $S_i \cap T^3 S_i$ or $S_i \cap T^2 S_i$ alone. The basic principle and fundamental difficulty involved in generating higher orders of permutation from the basic intersection $P(S_i \cap TS_i)$ in mixed systems are briefly discussed in the Appendix.

IV. PERMUTATIONAL REPRESENTATION AND PERIODIC ORBITS IN THE INTEGRABLE LIMIT: $\beta_{12}=0$

The phase space structure and po bifurcation analysis in the two Morse oscillator system coupled by a 1:1 resonant interaction is well understood.[20,22] The angle $\Psi_2=\frac{1}{2}(\theta_1+\theta_2)$ is ignorable, so that the conjugate variable $J_2=I_1+I_2$ is a constant of the motion. The existence of a constant of the motion in addition to the energy means that the system is integrable. We consider the integrable limit with $\beta_{12}=0$, and fixed $\beta_{11}=0.01$. In this integrable system, almost all pos occur in 1-parameter families on rational 2-tori (i.e., a torus for which the fundamental frequency ratio $\omega_1/\omega_2=m/n$). Thus, po ''bifurcation'' refers to the emergence of a new family of pos (rational torus) in the vicinity of an isolated po as the energy or coupling parameter changes. It should be noted that all rational tori intersect the S_1 and S_2 symmetry lines, so that the whole set of (marginally stable) pos exists on both symmetry lines in the integrable limit. As we shall see, understanding pos and their bifurcations in the integrable limit ($\beta_{12}=0$) provides the foundation for global analysis of po bifurcation for nonzero β_{12}. In this section, we show how permutational representations can be used to understand po organization on the sos Σ_1.

A. Bifurcation sequences for $S_1\cap TS_1$ and $S_2\cap TS_2$

Consider for example the case $\beta_{11}=0.01$, $\beta_{12}=0$ and $E=2.0$. For these parameter values, both symmetry lines S_1 and S_2 are intersected by their iterates at two points. The permutational representations are

$$P(S_1\cap TS_1)=\begin{pmatrix}1 & 2\\ 1 & 2\end{pmatrix} \tag{18}$$

and

$$P(S_2\cap TS_2)=\begin{pmatrix}1 & 2\\ 1 & 2\end{pmatrix}. \tag{19}$$

The corresponding periods are

$$\wp(P(S_1\cap TS_1))=(1_1,1_2) \tag{20}$$

and

$$\wp(P(S_2\cap TS_2))=(1_1,1_2). \tag{21}$$

The pair of fundamental (period 1) pos on S_1 is identical with the pair of fundamental pos on S_2. We refer to the orbit 1_1 as the *central periodic orbit* (cpo); it is a generalized local mode.[20] The orbit 1_2 is called the *primary resonant mode* (prm), and is a generalized normal or resonant mode.[20] Both orbits are stable, so that bifurcations of pos can occur on these orbits.

As the energy E increases, the pattern of intersections $P(S_1\cap TS_1)$ changes as follows

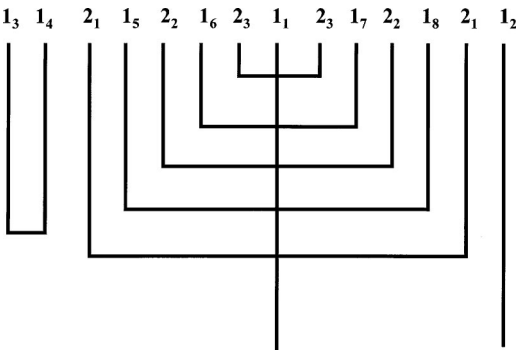

FIG. 4. Period-1 and period-2 pos on S_1 in the integrable limit. The diagram shows the relative location of pos on the symmetry line S_1 as a function of energy E, from low E (bottom of the figure) to high E (top). The coupling parameter $\beta_{12}=0$.

$$\begin{pmatrix}1 & 2\\ 1 & 2\end{pmatrix}_{E=2.0}\rightarrow\begin{pmatrix}3 & 2 & 1 & 4\\ 1 & 2 & 3 & 4\end{pmatrix}_{E=3.0}\rightarrow\begin{pmatrix}1 & 2 & 5 & 4 & 3 & 6\\ 1 & 2 & 3 & 4 & 5 & 6\end{pmatrix}_{E=4.0}. \tag{22}$$

The corresponding bifurcation sequences on S_1 are

$$(1_1,1_2)\rightarrow(2_1,1_1,2_1,1_2)\rightarrow(1_3,1_4,2_1,(1_1)^{\mathrm{cpo}},2_1,(1_2)^{\mathrm{prm}}), \tag{23}$$

where a family of period-2 rational tori first emerges from the local mode 1_1, $(2_1,1_1,2_1)$, followed by a saddle-center (tangent) bifurcation, $(1_3,1_4)$, where 1_3 and 1_2 are, respectively, stable and unstable pos (Fig. 4). The po 1_3 is another generalized local mode.

On S_2, the bifurcation sequence is

$$(1_1,1_2)\rightarrow(2_2,1_1,2_2,1_2)\rightarrow(1_3,1_4,2_2,1_1,2_2,1_2), \tag{24}$$

where another resonant period-2 bifurcation $(2_2,1_1,2_2)$ occurs. In the Appendix, it is shown that S_1 and S_2 have the same period-1, but not period-2, pos in common. Note that the two period-2 orbits 2_1 and 2_2 lie on the same rational torus. More generally, the appearance of a period-n orbit $(n>1)$ $(n_1,1_1,n_1)$ on the S_1 symmetry line is accompanied by the appearance of a complementary po $(n_2,1_1,n_2)$ on S_2, where the complementary po lies on the same rational torus. In the integrable limit, both pos are marginally stable; in the nonintegrable case ($\beta_{12}\neq 0$), one of the pos will be stable and the other unstable (see the discussion of pairing of pos in Sec. VII). For the integrable case, analysis of pos on S_1 alone suffices to determine po periods and actions.

So far we have examined bifurcation sequences numerically. Numerical construction of the bifurcation tree as a parameter such as E increases, although in principle straightforward, is unsatisfactory insofar as it is difficult to predict analytically which bifurcations will occur as a perturbation parameter increases (using, for example, normal form analysis[31]). In contrast, if a strongly chaotic limit exists for large values of the coupling parameter, for which a complete set of unstable pos can easily be enumerated, then one can formulate *pruning rules* governing the merging of orbits and

the appearance of stable pos as the coupling parameter is reduced. TJ have applied this approach to the Hénon map.[28] Such a ''reverse'' approach can be applied to (23), although in the coupled Morse oscillator system the strong coupling limit is by no means fully chaotic (hyperbolic). Once pruning patterns are established, possible po pruning sequences can be enumerated. Complications can arise if bifurcations occur in the reverse direction. For example, Schomerus[32] found that certain normal forms lead to po bifurcations followed by inverse bifurcations as a single parameter is varied; we have found such ''nonmonotonic'' behavior in the system examined here (see below). The TJ approach establishes the *global* structure of the po bifurcation diagram by revealing the po bifurcation or pruning patterns implicit in the topology of the intersections of the symmetry line and its iterates.

In any particular problem, additional information is usually required to decide between several possible allowed pruning sequences determined by the TJ approach. For example, in the reverse (pruning) direction in Eq. (23), we cannot determine the order in which the saddle-center bifurcation $(1_3,1_4)$ and the resonant period-2 bifurcation $(2_2,1_1,2_2)$ occur. In the next subsection we introduce the winding number assignment for pos as a ''pruning grammar'' that enables some possibilities to be eliminated.

B. Winding number assignments of pos

The permutational representation of pos specifies the periodicity m together with an additional index ℓ, where m is simply the number of distinct intersections of the po with the chosen sos (Σ_1, say). For the case of a continuous time system, as opposed to an area-preserving map,[28] it is important to have additional information on the nature of the po. The *winding number* for the po, m/n say, specifies a periodicity n in a complementary sos (Σ_3, say) in addition to m. In the integrable limit, the winding number is simply the ratio of fundamental frequencies on a given rational torus.

Close to the bifurcation point, two pos involved in a tangent (saddle-center) bifurcation must have the same number of intersections with any sos. Conversely, two pos with different winding numbers cannot merge in a tangent bifurcation; this constitutes a strict pruning rule. An analogous restriction also holds for other kinds of bifurcation e.g., island chain, in nonintegrable systems.

For example, the sequence of winding numbers for the bifurcation sequence (23) is

$$\begin{aligned}((1/1)^{\mathrm{cpo}},(1/1)^{\mathrm{prm}}) &\rightarrow (2/3,(1/1)^{\mathrm{cpo}},2/3,(1/1)^{\mathrm{prm}}) \\ &\rightarrow (1/1,1/1,2/3,(1/1)^{\mathrm{cpo}},2/3,(1/1)^{\mathrm{prm}}).\end{aligned} \tag{25}$$

Note that the sequence of numerators in (25) matches the period sequence (23) determined by permutation analysis on the sos Σ_1. The denominators, on the other hand, specify periodicities on sos Σ_3, so that the winding numbers provide a link between permutational representations on Σ_1 and Σ_3.

C. Permutational representations of pos for high energy

We now show how the order of pos on time-reversal symmetry lines can be enumerated and predicted. At the relatively high energy $E=6.98$ (the dissociation energy of the weakest bond is 8.0), there are 14 intersections for $S_1 \cap TS_1$ on the Σ_1 sos. The permutational representation is

$$P(S_1 \cap TS_1) = \begin{pmatrix} 1 & 2 & 13 & 4 & 11 & 6 & 9 & 8 & 7 \\ 1 & 2 & 3 & 4 & 5 & 6 & 7 & 8 & 9 \\ 10 & 5 & 12 & 3 & 14 & & & & \\ 10 & 11 & 12 & 13 & 14 & & & & \end{pmatrix}. \tag{26}$$

An important empirical observation is that the sum of adjacent numbers in the first row of the permutation (26) from the second column alternates between the values 15 and 17. The permutation (26) is said to have *indices* $\langle 15,17\rangle$.[28] Indices, when they exist, provide a compact specification of the structure of the intersection configuration.[28] (Note that there exists a set of indices for each order of permutation in the hyperbolic Hénon map. These indices can be used to generate permutations corresponding to arbitrary orders of iteration, $P(S_i \cap T^n S_i)$, $(n>1)$, from $P(S_i \cap TS_i)$.[28]) The permutation representation (26) also shows that there is symmetry around the cpo, $\binom{8}{8}$, which is manifested in the following sequence of periods [determined by the permutation (26)] [cf. (23)]:

$$\begin{aligned}&\wp(P(S_1 \cap TS_1)) \\ &\quad = (1_3,1_4,2_1,1_5,2_2,1_6,2_3,(1_1)^{\mathrm{cpo}},2_3,1_7,2_2,1_8,2_1,(1_2)^{\mathrm{prm}}).\end{aligned} \tag{27}$$

and winding numbers $\omega(P(S_1 \cap TS_1))$:

$$\begin{aligned}&(1/1_3,1/1_4,2/3_1,1/2_5,2/5_2,1/3_6,2/7_3,(1/1_1)^{\mathrm{cpo}}2/7_3,1/3_7, \\ &\quad 2/5_2,1/2_8,2/3_1,(1/1_2)^{\mathrm{prm}}),\end{aligned} \tag{28}$$

where the subscript distinguishes between orbits having the same periodicity. The winding number sequence (28) shows that the winding numbers (n/m) on the left side of the cpo between $1/1_4$ and $(1/1_1)^{\mathrm{cpo}}$ decrease monotonically as the cpo is approached, and then increase monotonically to the right (up to $(1/1_2)^{\mathrm{prm}}$). On the Σ_1 ($\theta_2=0$) sos, the symmetry line S_1 is the line $p_1=0$, which consists of two branches: $\theta_1=0$, corresponding to $q_1 \geqslant 0$, and $\theta_1=\pi$, corresponding to $q_1 \leqslant 0$. The cpo is an orbit of minimal action $I_1 \simeq 0$ and maximal action I_2; the action I_1 therefore increases as we move way from the cpo on either side, and the behavior of the winding numbers follows from the negative mode anharmonicities ($\alpha_i>0$). Moreover, as we shall show, the ordering of winding numbers can be understood using a Farey tree construction.[33]

For the local mode $1/1_3$, winding numbers (n/m) on the left side of the cpo between $1/1_3$ and $(1/1_1)^{\mathrm{cpo}}$ decrease monotonically towards the cpo. On the Σ_3 ($\theta_1=0$) sos, the local mode $1/1_3$ is at the center with minimal action I_2 and

maximal action I_1. The winding numbers are flipped, i.e., m/n, and monotonically decrease towards $1/1_3$.

At the same energy there are 26 intersections at the second iteration, $S_1 \cap T^2 S_1$, with indices $\langle 27,29 \rangle$. The permutational representation is

$$P(S_1 \cap T^2 S_1) = \begin{pmatrix} 1 & 26 & 3 & 24 & 5 & 22 & 7 & 20 & 9 & 18 \\ 1 & 2 & 3 & 4 & 5 & 6 & 7 & 8 & 9 & 10 \\ 11 & 16 & 13 & 14 & 15 & 12 & 17 & 10 & & \\ 11 & 12 & 13 & 14 & 15 & 16 & 17 & 18 & & \\ 19 & 8 & 21 & 6 & 23 & 4 & 25 & 2 & & \\ 19 & 20 & 21 & 22 & 23 & 24 & 25 & 26 & & \end{pmatrix}, \quad (29)$$

The 14 pos of (27) have period 1 or 2, and so appear in 14 cycles of length 1 in $P(S_1 \cap T^2 S_1)$. The period sequence $\wp(P(S_1 \cap T^2 S_1))$ in (29) is then determined uniquely:

$$(1_3,4_1,1_4,4_2,2_1,4_3,1_5,4_4,2_2,4_5,1_6,4_6,2_3,(1_1)^{\mathrm{cpo}},2_3,4_6,$$
$$1_7,4_5,2_2,4_4,1_8,4_3,2_1,4_2,(1)^{\mathrm{prm}},4_1). \quad (30)$$

The winding number sequence $\omega(P(S_1 \cap T^2 S_1))$ is

$$(1/1_3,4/3_1,1/1_4,4/5_2,2/3_1,4/7_3,1/2_5,4/9_4,2/5_2,4/11_5,$$
$$1/3_6,4/13_6,2/7_3,(1/1_1)^{\mathrm{cpo}}, \quad 2/7_3,4/13_6,1/3_7,4/11_5,2/5_2,$$
$$4/9_4,1/2_8,4/7_3,2/3_1,4/5_2,(1/1_2)^{\mathrm{prm}},4/3_1). \quad (31)$$

There are 38 intersections for $S_1 \cap T^3 S_1$ with indices $\langle 39,41 \rangle$. The permutation is given by

$$P(S_1 \cap T^3 S_1) = \begin{pmatrix} 1 & 2 & 37 & 4 & 35 & 6 & 33 & 8 & 31 & 10 & 29 & 12 \\ 1 & 2 & 3 & 4 & 5 & 6 & 7 & 8 & 9 & 10 & 11 & 12 \\ 27 & 14 & 25 & 16 & 23 & 18 & 21 & 20 & 19 & 22 & 17 & \\ 13 & 14 & 15 & 16 & 17 & 18 & 19 & 20 & 21 & 22 & 23 & \\ 24 & 15 & 26 & 13 & 28 & 11 & 30 & 9 & & & & \\ 24 & 25 & 26 & 27 & 28 & 29 & 30 & 31 & & & & \\ 32 & 7 & 34 & 5 & 36 & 3 & 38 & & & & & \\ 32 & 33 & 34 & 35 & 36 & 37 & 38 & & & & & \end{pmatrix}. \quad (32)$$

Periodicities for the 1-cycles (unit column) are either 1 or 3, and for the 2-cycles either 2 or 6. Knowledge of the permutation (32) is not sufficient to determine the location of period 1 versus 3 (or 2 versus 6) pos in the sequence. One possible way to assign periodicities is to analyze the bifurcation sequences associated with each possible configuration.[28] Here, in the integrable limit, we use the Farey tree organization of the winding numbers to determine the periods.

In a region of the symmetry line where winding numbers increase or decrease monotonically, pos with winding numbers (j/k) and (ℓ/m) have lying between them a po of winding number $(j+\ell)/(k+m)$, where the new winding number is obtained by Farey addition (add numerators and denominators).[33]

The symmetry of the cycle structure in (32) shows that the 1-cycle $\binom{20}{20}$ is the cpo $(1/1)^{\mathrm{cpo}}$. Consider winding numbers of the first four columns in (32). Due to the monotonic increase of winding numbers towards $1/1_3$, the period-3 po 3/2, represented by a 1-cycle in $P(S_1 \cap T^3 S_1)$, will appear between $1/1_3$ and $4/3_1$ in (31). Farey addition of winding numbers between $3/2_1$ and $1/1_4$ leads to the po sequence 4/3, 5/4, 6/5,.... The unit column $\binom{2}{2}$ therefore corresponds to period-3, $\binom{37}{3}$ and $\binom{4}{4}$ are period six and period one, respectively. Similarly, period-3 pos between $\binom{4}{4}$ and $\binom{20}{20}$ can be located by Farey addition of winding numbers from (28) and (31):

$$1/1,3/2,1/1,3/4,2/3,3/5,1/2,3/7,2/5,3/8,1/3,3/10,2/7,(1/1)^{\mathrm{cpo}},2/7,3/10,1/3,3/8,2/5,3/7,1/2,3/5,2/3,3/4,(1/1)^{\mathrm{prm}},3/2. \quad (33)$$

From (33), the winding number sequence $\omega(PS_1 \cap T^3 S_1)$ is then

$$(1/1_3,3/2_1,6/5_1,1/1_4,6/7_2,3/4_2,2/3_1,3/5_3,6/11_3,1/2_5,6/13_4,3/7_4,2/5_2,3/8_5,6/17_5,1/3_6,6/19_6,3/10_6,2/7_3,(1/1_1)^{\mathrm{cpo}},$$
$$2/7_3,3/10_7,6/19_6,1/3_7,6/17_5,3/8_8,2/5_2,3/7_9,6/13_4,1/2_8,6/11_3,3/5_{10},2/3_1,3/4_{11},6/7_2,(1/1_2)^{\mathrm{prm}},6/5_1,3/2_{12}). \quad (34)$$

Inserting period-4 pos into the winding number sequence (34) we construct the union of winding number sequences, (28), (31), and (34):

$$\cup_{i=1}^{3} \omega(P(S_1 \cap T^i S_1)) = (1/1,3/2,4/3,6/5,1/1,6/7,4/5,3/4,2/3,3/5,4/7,6/11,1/2,6/13,4/9,3/7,2/5,3/8,4/11,6/17,1/3,$$
$$6/19,4/13,3/10,2/7,(1/1)^{\mathrm{cpo}},2/7,3/10,4/13,6/19,1/3,6/17,4/11,3/8,2/5,3/7,4/9,6/13,1/2,6/11,$$
$$4/7,3/5,2/3,3/4,4/5,6/7,(1/1)^{\mathrm{prm}},6/5,4/3,3/2). \quad (35)$$

For higher order permutations $P(S_1 \cap T^i S_1)$, $(i \geq 4)$, 2-cycles (pairs of columns) appear near $(1/1)^{\text{prm}}$. For example, in $P(S_1 \cap T^4 S_1)$, which has 52 intersections, a period-8 po with winding number 8/8 appears in the vicinity of the prm $(1/1)^{\text{prm}}$

$$P(S_1 \cap T^4 S_1) = \begin{pmatrix} & 49 & 48 & 47 & \\ \ldots, & & & & ,\ldots \\ & 47 & 48 & 49 & \end{pmatrix}, \tag{36}$$

where $(1/1)^{\text{prm}}$ corresponds to $\binom{48}{48}$ and the period-8 to the 2-cycle $\binom{49\ 47}{47\ 49}$. From (36), one can see also that the permutation no longer has good indices $\langle 53,55 \rangle$ due to the occurrence of the third pruning center $(1/1)^{\text{prm}}$.

It is interesting to note that frequency ratios (winding numbers) are constant in the 1:1 resonance region (i.e., all have winding numbers $m/m=1$). Constant frequency ratios in resonance zones were found by Laskar using local frequency analysis of near-integrable systems.[34]

By continued Farey addition, winding number sequences can be constructed for any order of iteration, where winding numbers in the 1:1 resonant region in the vicinity of $(1/1)^{\text{prm}}$ are constant.

V. PRUNING PATTERNS OF POS

In a mixed system, regular and irregular regions are interleaved in phase space in an extremely intricate manner.[3] As a result, high-order iterates of the symmetry line can have very complicated shapes, and it is difficult to determine po bifurcation patterns as system parameters change (from the high energy limit, for example) by considering all possible deformations of the iterated symmetry line. It is however possible to construct possible global bifurcation diagrams by finding *pruning* (bifurcation) patterns at the pruning (bifurcation) points for the pos on the symmetry lines. Once the possible pruning patterns are determined, it is straightforward to construct pruning (bifurcation) sequences. This is accomplished by starting with the order of the pos on the symmetry lines for some energy and finding where the pruning patterns appear in the periodic sequence. Those pos in the patterns are then pruned, and the process continued at the next level. In this way, one can see how retreat from the fully chaotic limit occurs (for systems such as the Hénon map[28]), and in the process construct global bifurcation diagrams.

For the system of coupled Morse oscillators under study here, we find two relevant pruning patterns (see Fig. 5). The first (called type *I*) involves three sequential intersection points (n_i, m, n_j), such as an island-chain type bifurcation $(k=n/m \in N)$ or a period-doubling type bifurcation $(n/m=2)$. In a type *I* pattern, two points (n_i, n_j) are pruned at the pruning center, m. This pattern can be understood as follows: if local analysis (such as a normal form[5]) indicates that the local functional behavior of the iterate follows (generically) a cubic polynomial, then two of the three roots, (n_i, n_j) become degenerate or complex conjugate at the bifurcation point. Note that, if $i \neq j$, that is, if the two points (n_i, n_j) are different pos, a pair of identical pruning events (n_i, m, n_j) occurs at exactly the same parameter value. It is important to note that, for the $i \neq j$ case, the pruning center m must be part of a 2-cycle in the permutation in order to have a pair of identical pruning events; otherwise the sequence (n_i, m, n_j) is not a pruning sequence. Furthermore, in the type *I* pattern, the period-m po is necessarily stable just after pruning. Stability of the orbit is indicated by superscript s, m^s.

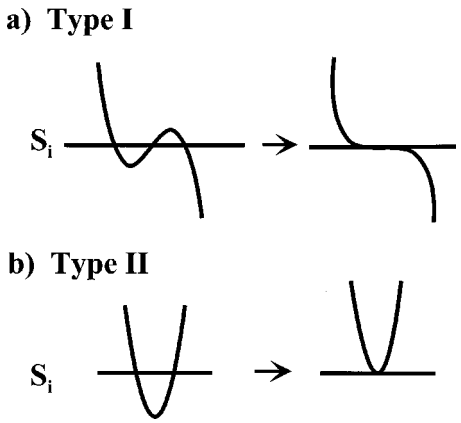

FIG. 5. Two basic pruning patterns for the coupled Morse system. The diagram shows two essentially different ways in which the pattern of intersections of a symmetry line S_i and its iterate can undergo qualitative change with variation in system parameter. (a) Type *I* pruning. This case corresponds to either an island-chain or a period-doubling bifurcation. (b) Type *II* pruning. This case corresponds to tangent bifurcation.

The second pruning pattern (type *II*) involves two adjacent intersection points (n_i, n_j). Here, the two points (n_i, n_j) are pruned at the same time. If $i \neq j$, a pair of identical pruning events occurs at the same parameter value. The type *II* bifurcation is a *tangent bifurcation*. Tangent bifurcation can occur whenever two pos of the same period appear as two adjacent columns, $(\cdots \overset{j}{i}\ \overset{j+1}{i+1} \cdots)$. The local functional behavior is (generically) quadratic, so that two real solutions become complex conjugate after pruning/prior to bifurcation. According to the Poincaré–Birkhoff theorem,[3] a stable and unstable po pair is pruned in the type *II* case.

Note that the pruning sequence of the so-called *touch-and-go* bifurcation[5,11] (n_1, m, n_2), $(k=n/m \in N$ for $k=3l)$, $(n_1, m, n_2) \rightarrow (n_1, n_2, m)$ or $(m, n_1, n_2) \rightarrow (m)$, is considered to be a special case of the type *I* pruning. In the rest of this paper, we show how the origin of ubiquitous tangent bifurcations seen upon turning on the nonintegrability parameter β_{12} can be understood in terms of type *I* and *II* pruning patterns.

VI. GLOBAL BIFURCATION ANALYSIS

The existence of *pruning degeneracy*[28] means that several different possible sequences of bifurcations are possible starting from a given periodic sequence. In order to narrow the range of possibilities, we introduce winding number assignments for pos. For the nonintegrable case, this assignment is based on the number of intersections with sos defined by the two fundamental pos (see below). By eliminating possible tangency problems (see below), we ensure that type *I* and *II* pruning (bifurcation) can only occur for pos with the same winding number.

A. Bifurcations for the integrable system

1. Pruning sequence for $P(S_1 \cap TS_1)$

For the winding number sequence (28) associated with the first iterate of S_1, the full pruning sequence ending with (25) is

$$
\begin{array}{c}
(1/1_3,1/1_4,2/3_1,1/2_5,2/5_2,1/3_6,\underline{2/7_3},(1/1_1)^{\mathrm{cpo}},\underline{2/7_3},1/3_7,2/5_2,1/2_8,2/3_1,(1/1_2)^{\mathrm{prm}}) \\
\downarrow \\
(1/1_3,1/1_4,2/3_1,1/2_5,2/5_2,\underline{1/3_6},(1/1_1)^{\mathrm{cpo}},\underline{1/3_7},2/5_2,1/2_8,2/3_1,(1/1_2)^{\mathrm{prm}}) \\
\downarrow \\
(1/1_3,1/1_4,2/3_1,1/2_5,\underline{2/5_2},(1/1_1)^{\mathrm{cpo}},\underline{2/5_2},1/2_8,2/3_1,(1/1_2)^{\mathrm{prm}}) \\
\downarrow \\
(1/1_3,1/1_4,2/3_1,\underline{1/2_5},(1/1_1)^{\mathrm{cpo}},\underline{1/2_8},2/3_1,(1/1_2)^{\mathrm{prm}}) \\
\downarrow \\
(\underline{1/1_3},\underline{1/1_4},2/3_1,(1/1_1)^{\mathrm{cpo}},2/3_1,(1/1_2)^{\mathrm{prm}}) \\
\downarrow \\
(\underline{2/3_1},(1/1_1)^{\mathrm{cpo}},\underline{2/3_1},(1/1_2)^{\mathrm{prm}}) \\
\downarrow \\
((1/1_1)^{\mathrm{cpo}},(1/1_2)^{\mathrm{prm}})
\end{array}
\tag{37}
$$

where pos to be pruned are underlined. Pruning degeneracy between $(1/1_3,1/1_4)$ and $(2/3_1,(1/1_1)^{\mathrm{cpo}},2/3_1)$ occurs in the above pruning sequence (37) (see below).

2. Three pruning centers in the integrable limit

The pruning sequence for the winding numbers (31) associated with the second iterate of S_1, T^2S_1, shows that there are two ''pruning centers.'' One of the pruning sequences is shown below.

$$
\begin{array}{c}
((1/1)_3^{\mathrm{spc}},4/3_1,1/1_4,4/5_2,2/3_1,4/7_3,1/2_5,4/9_4,2/5_2,4/11_5,1/3_6,4/13_6,\underline{2/7_3}, \\
(1/1_1)^{\mathrm{cpo}},\underline{2/7_3},4/13_6,1/3_7,4/11_5,2/5_2,4/9_4,1/2_8,4/7_3,2/3_1,4/5_2,(1/1_2)^{\mathrm{prm}},4/3_1) \\
\downarrow \\
\text{pruning at the cpo} \\
\downarrow \\
((1/1)_3^{\mathrm{spc}},\underline{4/3_1},1/1_4,4/5_2,2/3_1,(1/1_1)^{\mathrm{cpo}},2/3_1,4/5_2,(1/1_2)^{\mathrm{prm}},\underline{4/3_1}) \\
\downarrow \\
\text{pruning at the spc} \\
\downarrow \\
(\underline{1/1_3},\underline{1/1_4},4/5_2,2/3_1,(1/1_1)^{\mathrm{cpo}},2/3_1,4/5_2,(1/1_2)^{\mathrm{prm}}) \\
\downarrow \\
\vdots \\
\downarrow \\
((1/1_1)^{\mathrm{cpo}},(1/1_2)^{\mathrm{prm}}),
\end{array}
\tag{38}
$$

where one center is the cpo and the other center is the $1/1_3$ orbit, called the *second pruning center* (spc). In order to have the tangent bifurcation of pos $((1/1)_3^{\mathrm{spc}},1/1_4)$ shown in (37) for the winding number sequence (35), the two $4/3_1$ pos, one between $((1/1)^{\mathrm{spc}},1/1)$ and the other to the right of the resonant mode $(1/1)^{\mathrm{prm}}$, have to be pruned at the spc. The primary resonant mode $(1/1)^{\mathrm{prm}}$ therefore acts as a ''stopper'' for pruning these three orbits at the cpo.

The above pruning sequence (38) exhibits pruning degeneracy.[28] Additional information is required to determine the order of prunings at the two centers. Thus, we cannot predict when the orbit $4/3_1$ is pruned at the spc relative to po prunings at the cpo. Nevertheless, the order of prunings at each center can be determined uniquely.

We can now construct the pruning sequence for the union of the winding numbers (35) up to the third iterate, T^3S_1. We reorder the winding numbers (35) to highlight the pruning order of pos at the two pruning centers:

(1) Pruning at the cpo,

$$(6/7,4/5,3/4,2/3,3/5,4/7,6/11,1/2,6/13,4/9,3/7,2/5,$$
$$3/8,4/11,6/17,1/3,6/19,4/13,3/10,2/7,(1/1)^{\mathrm{cpo}},2/7,$$
$$3/10,4/13,6/19,1/3,6/17,4/11,3/8,2/5,3/7,4/9,6/13,$$
$$1/2,6/11,4/7,3/5,2/3,3/4,4/5,6/7). \quad (39)$$

(2) Pruning at the spc,

$$(6/5,4/3,3/2,(1/1)^{\mathrm{spc}},3/2,4/3,6/5,1/1). \quad (40)$$

The stable primary resonant mode $(1/1)^{\mathrm{prm}}$ acts as a third pruning center for 2-cycles centered at the prm; these appear for higher order iterations, $P(S_1 \cap T^i S_1)$, $i \geq 4$ [see Eq. (36)].

As shown above, there are three pruning groups: the first group is related to the spc, $(1/1)^{\mathrm{spc}}$, the second group to the cpo, $(1/1)^{\mathrm{cpo}}$, and the third to the prm, $(1/1)^{\mathrm{prm}}$. The number of pos created around those centers at each order of iteration is in general different on each sos. In the rest of the paper we focus on the three pruning groups independently.

B. Nonintegrable system ($\beta_{12} \neq 0$): tangency and two-parameter (codimension-2) bifurcations

Once the second coupling parameter β_{12} becomes nonzero, all rational tori break up into stable and unstable pos via Poincaré-Birkhoff island-chain type bifurcation. (The islands associated with high-order resonances may be very small, however.[24]) The coupled Morse system now exhibits locally chaotic motion. The polyad number,[35] $J_2 = I_1 + I_2$, ceases to be an invariant, and regular and chaotic components coexist in an extremely complicated manner in phase space.

Classical po energy-period (E, τ) plots for integrable and nonintegrable cases are shown in Fig. 6. The (E, τ) plot for the integrable limit exhibits a rich structure. Such structure is well understood;[13] each trace in the (E, τ) plot corresponds either to a rational 2-torus (1-parameter family of pos) or an isolated po,[13] and repetitions thereof. In the integrable limit [Fig. 6(a)], the tangent bifurcation creating the po pair 1_3 and 1_4 is an important feature of the plot. Rational tori appear by bifurcating off isolated (stable) po traces. The corresponding (E, τ) plot for the system with nonintegrable perturbation [Fig. 6(b)] is very similar in overall structure to that of the integrable case, up to the maximum times considered. Detailed comparison shows that onset of nonintegrability is associated with the appearance of ubiquitous tangent bifurcations derived from the bifurcation structure for the integrable limit [(39) and (40)]. As explained below, these tangent bifurcations emerge from the integrable limit by a mechanism involving a codimension-2 bifurcation, i.e., an essentially 2-parameter scenario. Codimension-2 bifurcations have received relatively little attention (for recent work, see Refs. 31 and 32).

As already mentioned, the system of coupled Morse oscillators under study is not strictly hyperbolic in the limit of high energy or large coupling parameter. We shall analyze the evolution of po sequences from the integrable limit

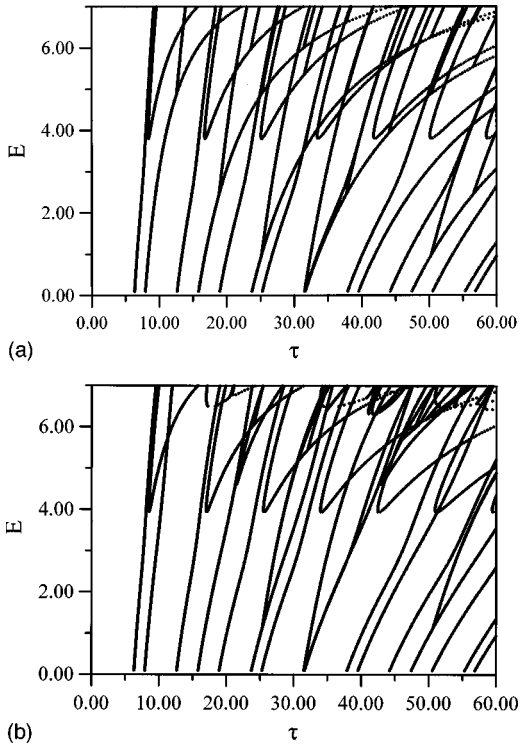

FIG. 6. Classical (E, τ) plots for coupled Morse oscillators, $\beta_{11} = 0.01$. Traces are associated with either isolated pos or rational tori, and repetitions. (a) $\beta_{12} = 0$, integrable limit. The tangent bifurcation creating the po pair $(1_3, 1_4)$ is an important feature of this plot. (b) $\beta_{12} = 0.022$, nonintegrable case. This plot differs from the integrable case by the presence of many additional tangent bifurcations involving high-order pos.

($\beta_{11} \neq 0$, $\beta_{12} = 0$) as the coupling parameter β_{12} increases at fixed energy ($E = 6.98$). In this way, the route to tangent bifurcations is revealed.

1. Winding number assignments in the nonintegrable case

The winding number assignment depends on the sos pair used. One problem with using a pair of complementary sos such as Σ_1 and Σ_3, as done in the integrable case, is the possibility that a po might become tangent to one of the sos, leading to a discontinuous change in winding number (as a function of E, for example). We can however use the two fundamental pos discussed above, 1^{cpo} and 1^{prm}, to define two new dynamically determined sos, denoted Ξ_1 and Ξ_2, and so avoid the tangency problem.[36] Tangency of any po to the fundamental pos is forbidden (unless this orbit is involved in a bifurcation with the fundamental pos), and so all pos must intersect both sos Ξ_i defined by trajectory crossings of the fundamental pos in configuration space. New coordinates (ξ_i, η_i), $i = 1,2$, are defined by the perpendicular distance (η_i) from the fundamental orbit i and the position (ξ_i) of intersections on the fundamental po, where we take the origin $\xi_i = 0$ to lie on the time-reversal mirror $\mathcal{M}$. The sos Ξ_i are then defined by $\eta_i = 0$ and $\dot{\xi}_i \geq 0$. A winding number n/m is obtained from the number of intersections with the fundamental pos with $\dot{\xi}_i \geq 0$, where n and m are the number of intersections with 1^{cpo} and 1^{prm}, respectively; that is, the number of points on the two sos Ξ_i. It is important to

note that the winding number of pos bifurcating from the fundamental pos corresponds to the periodicity of pos on the dynamical sos Ξ_i, $(i=1,2)$, and is an invariant quantity characterizing the po. The numerator for such pos agrees with the period determined by the permutational analysis. For pos that do not bifurcate from the fundamental pos, the numerator of the winding number is in general not equal to the periodicity on Σ_1. In the integrable limit, both winding number assignments become equivalent. In the nonintegrable case, however, winding numbers no longer vary monotonically along the symmetry line,[34] and the Farey tree structure is disrupted.

2. Abrupt change in the position of the cpo

For $\beta_{12}=0.0003$ and $E=6.98$, the permutational representation for $S_1 \cap TS_1$ is the same as that for the integrable system (26). The winding number sequence is however

$$((1/1_3)^{\mathrm{spc}}, 1/1_4, 2/3_1, 1/2_5, 2/4_2, 1/2_6, 2/4_3, (1/2_7)^c, 2/4_3, 1/2_8, 2/4_2, (1/1_1)^{\mathrm{cpo}}, 2/3_1, (1/1_2)^{\mathrm{prm}}). \quad (41)$$

The relative position of the (1/1) cpo on the symmetry line changes abruptly, so that the winding number sequence is different from that of (28), and the po sequence now exhibits symmetry about the po $(1/2_7)^c$, which appears at the previous location of the cpo. The sos Σ_1 $(E=5.0)$ for both the integrable $(\beta_{12}=0)$ and the nonintegrable case $(\beta_{12}=0.0003)$ is shown in Fig. 7.

The winding number sequence clearly shows that the pruning sequence must involve tangent bifurcations of the 1/2 orbits, as all of the 1/2 orbits cannot be created via type *I* bifurcations. Since β_{12} is small, a drastic change in the pruning sequence from that of the integrable system, (37), is not expected. The first pruning group is just the tangent bifurcation $(1/1_3, 1/1_4)$. For these parameter values, no bifurcation appears in the third group at the first iteration. Pruning sequences are shown below for the second group. We remark that the pruning analysis for the sequence of periods (27) shows *all* possible pruning (or bifurcation) sequences, including that for (41), that are inherent in the topology of the configuration of the intersections.

There are two possible prunings for the period-1/2 orbits in the second group:

(1) One tangent (1/2,1/2) bifurcation:

$$\begin{array}{c}
(2/3_1, 1/2_5, 2/4_2, 1/2_6, \underline{2/4_3}, (1/2_7^s)^c, \underline{2/4_3}, 1/2_8, 2/4_2, (1/1_1)^{\mathrm{cpo}}, 2/3_1, (1/1_2)^{\mathrm{prm}}) \\
\downarrow \\
(2/3_1, 1/2_5, 2/4_2, \underline{1/2_6}, (1/2_7^s)^c, \underline{1/2_8}, 2/4_2, (1/1_1)^{\mathrm{cpo}}, 2/3_1, (1/1_2)^{\mathrm{prm}}) \\
\downarrow \\
(2/3_1, 1/2_5, \underline{2/4_2}, (1/2_7^s)^c, \underline{2/4_2}, (1/1_1)^{\mathrm{cpo}}, 2/3_1, (1/1_2)^{\mathrm{prm}}) \\
\downarrow \\
(2/3_1, (\underline{1/2_5^u}, (\underline{1/2_7^s})^c), (1/1_1)^{\mathrm{cpo}}, 2/3_1, (1/1_2)^{\mathrm{prm}}) \\
\downarrow \\
(\underline{2/3_1}, (1/1_1^s)^{\mathrm{cpo}}, \underline{2/3_1}, (1/1_2)^{\mathrm{prm}}) \\
\downarrow \\
((1/1_1^s)^{\mathrm{cpo}}, (1/1_2)^{\mathrm{prm}}).
\end{array} \quad (42)$$

(2) Two tangent (1/2,1/2) bifurcations:

$$\begin{array}{c}
(2/3_1, 1/2_5, 2/4_2, 1/2_6, \underline{2/4_3}, (1/2_7^s)^c, \underline{2/4_3}, 1/2_8, 2/4_2, (1/1_1)^{\mathrm{cpo}}, 2/3_1, (1/1_2)^{\mathrm{prm}}) \\
\downarrow \\
(2/3_1, 1/2_5, 2/4_2, \{(\underline{1/2_6^u}, (\underline{1/2_7^s})^c), 1/2_8, \ \text{or} \ 1/2_6, ((\underline{1/2_7^s})^c, \underline{1/2_8^u})\}, 2/4_2, (1/1_1)^{\mathrm{cpo}}, 2/3_1, (1/1_2)^{\mathrm{prm}}) \\
\downarrow \\
(2/3_1, 1/2_5, \underline{2/4_2}, 1/2^s_{6,\ \text{or}\ 8}, \underline{2/4_2}, (1/1_1)^{\mathrm{cpo}}, 2/3_1, (1/1_2)^{\mathrm{prm}}) \\
\downarrow \\
(2/3_1, (\underline{1/2_5^u}, \underline{1/2^s_{6,\ \text{or}\ 8}}), (1/1_1)^{\mathrm{cpo}}, 2/3_1, (1/1_2)^{\mathrm{prm}}) \\
\downarrow \\
(\underline{2/3_1}, (1/1_1^s)^{\mathrm{cpo}}, \underline{2/3_1}, (1/1_2)^{\mathrm{prm}}) \\
\downarrow \\
((1/1_1^s)^{\mathrm{cpo}}, (1/1_2)^{\mathrm{prm}}),
\end{array} \quad (43)$$

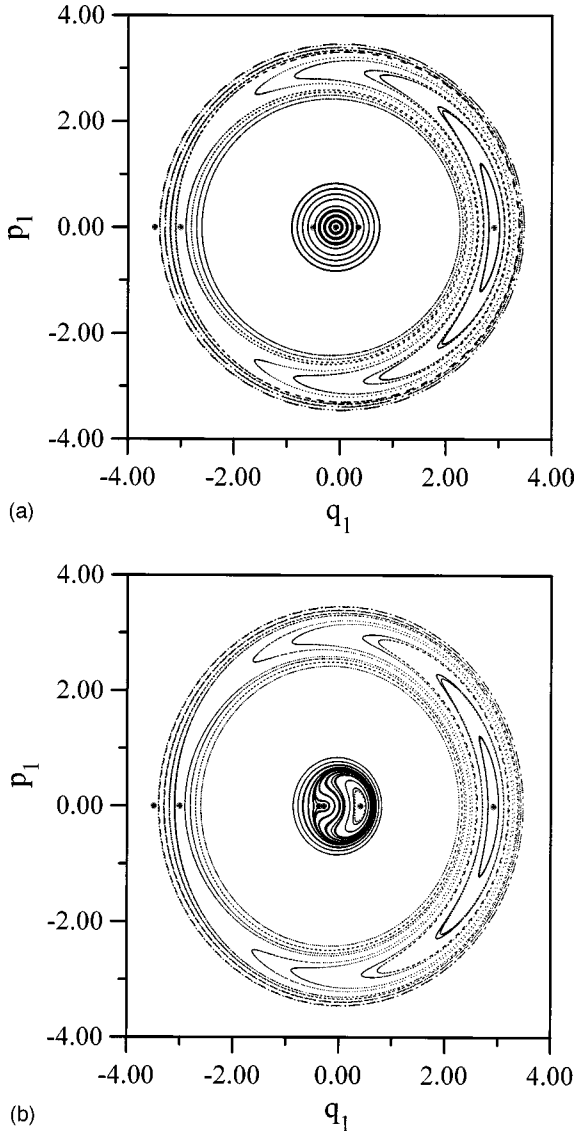

FIG. 7. Surface of section Σ_1 for the coupled Morse system, where Σ_1 is defined by the condition $\Sigma_1 \equiv \{\theta_2 = 0,\ \dot{\theta}_2 \geq 0\}$. Period-1 pos on the symmetry line $p_1 = 0$ are shown as filled circles. Energy $E = 5.0$. (a) $\beta_{12} = 0.0$. (b) $\beta_{12} = 0.0003$. Tangent bifurcation of pos 1_5 and 1_7. Note the reordering of the central pos on the symmetry line as the nonintegrable perturbation is turned on.

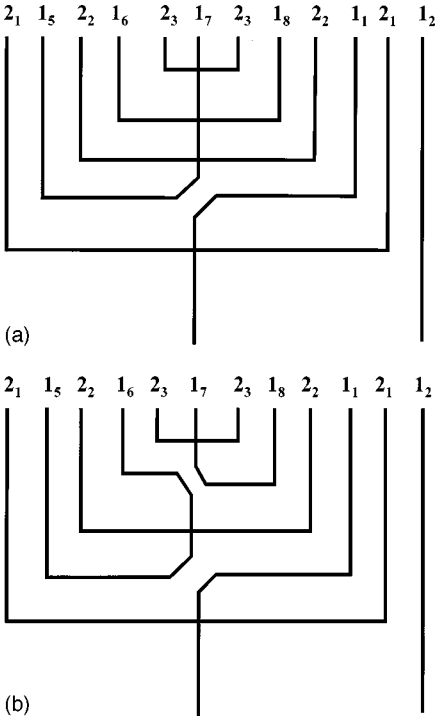

FIG. 8. Schematic bifurcation analysis for $S_1 \cap TS_1$. The relative ordering of period-1 and period-2 pos on the symmetry line S_1 is shown as a function of energy for fixed parameters $\beta_{11} = 0.01$ and β_{12}. Both sequences shown are found numerically. (a) $\beta_{12} = 0.0003$ [cf. Eq. (42)]. Note that the reordering of the three middle period-1 pos on the symmetry line seen in Fig. 7(b) occurs as a consequence of the ''disconnection'' of the pos 1_5, 1_1 and 1_8 (cf. Fig. 4). (b) $\beta_{12} = 0.015$ [cf. Eq. (43)]. Another disconnection involving pos 1_6, 1_1 and 1_7 is seen (cf. Fig. 4).

where two possible prunings for the tangent bifurcation of the 1/2 orbits are shown inside the curly brackets: ''left tangency'' $(\ldots, \underline{1/2}_6, (\underline{1/2}_7)^c, 1/2_8, \ldots)$ or ''right tangency'' $(\ldots, 1/2_6, (\underline{1/2}_7)^c, \underline{1/2}_8, \ldots)$.

Bifurcation diagrams for (42) and (43) are shown in Fig. 8. Numerically, the pruning sequence (42) with one tangent bifurcation (1/2,1/2) occurs as energy E varies with $\beta_{12} = 0.0003$, while the sequence (43) with right tangency occurs for higher values of β_{12} (see Fig. 8, $\beta_{12} = 0.015$), so that the po 1_8 is unstable $(1/2_8^u)$ and the po 1_6 is stable $(1/2_6^s)$. As a general rule, we find that, as the coupling parameter β_{12} increases, so does the number of tangent bifurcations. In a pair of pos involved in a tangent bifurcation, one is stable and the other is unstable. For instance, the po $1/2_6^s$ is stable, so that the existence of a tangent bifurcation $(1/2_5, 1/2_6^s)$ means that the po $1/2_5$ must be unstable, $1/2_5^u$. The period-1 po stabilities are therefore

$$(1/1_3^s, 1/1_4^u, 1/2_5^u, 1/2_6^s, (1/2_7^s)^c, 1/2_8^u, (1/1_1^s)^{\mathrm{cpo}}, (1/1_2^s)^{\mathrm{prm}}). \tag{44}$$

Note that a change in stability of period-1 pos from unstable to stable is not observed in the coupled Morse system for energies below $E = 7.0$.

The mechanism of onset of tangency for period-1 pos is disconnection of the two period-1 orbits from the (integrable) bifurcation tree, (37) (see Fig. 9; cf. also the work of Weston and Child[29]). As we shall see below, onset of tangency for higher-order pos follows a different route.

It is important to note that the period-2 orbits in the sequence (41) *cannot* undergo tangent bifurcations. The period-1 orbits are sandwiched between the period-2 pos, and so act as stoppers for tangent bifurcations of the period-2 pos. New period-2 orbits (or more period-1 orbits) need to appear in the sequence in order to see tangencies of the period-2 orbits. *This is the first example where the structure of the period sequence determines which pruning sequence is possible.* We show below that the mechanism by which tangent bifurcations of period-n orbits ($n \geq 2$) appear is different from that for period-1 orbits. Moreover, analysis of the intersection $S_1 \cap T^2 S_1$ ($\beta_{12} = 0.02$ and $E = 6.98$) reveals that the onset of tangency of period-2 pos is correlated with the tangency of period-4 orbits (see below).

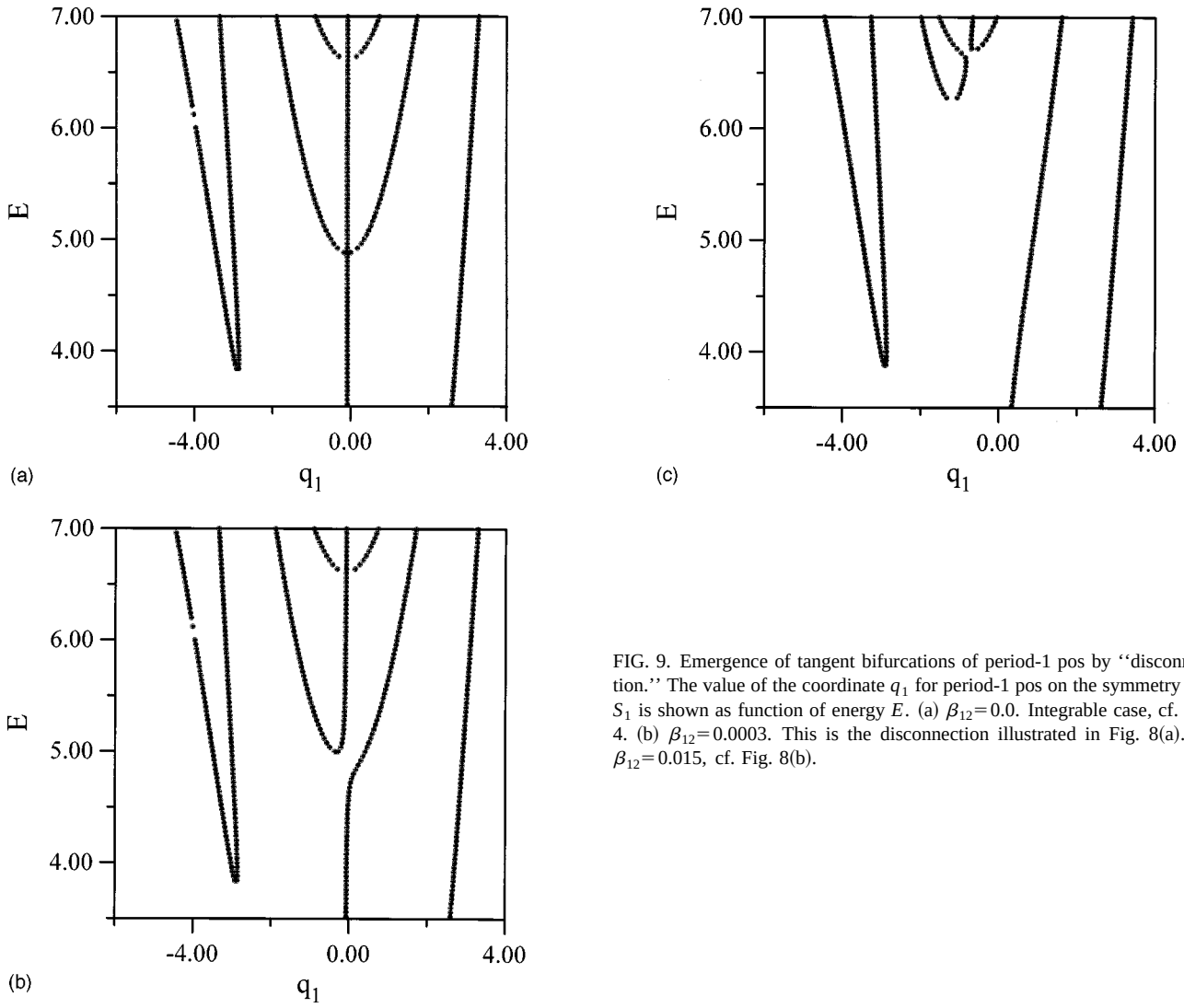

FIG. 9. Emergence of tangent bifurcations of period-1 pos by ''disconnection.'' The value of the coordinate q_1 for period-1 pos on the symmetry line S_1 is shown as function of energy E. (a) $\beta_{12}=0.0$. Integrable case, cf. Fig. 4. (b) $\beta_{12}=0.0003$. This is the disconnection illustrated in Fig. 8(a). (c) $\beta_{12}=0.015$, cf. Fig. 8(b).

3. Tangency for period-2 bifurcations: collision of period-2 bifurcations

As β_{12} is increased at fixed E, the number of pos increases. The number of pos for $S_1 \cap TS_1$ with $\beta_{12}=0.02$ and $E=6.98$ increases from 14 [see (26)] to 16. An increase in the number of intersections is associated with the creation of a new period-2 orbit. The permutational representation for $S_1 \cap TS_1$ is

$$P(S_1 \cap TS_1)=\begin{pmatrix} 1 & 2 & 15 & 4 & 11 & 6 & 9 & 8 & 7 \\ 1 & 2 & 3 & 4 & 5 & 6 & 7 & 8 & 9 \\ 10 & 5 & 14 & 13 & 12 & 3 & & 16 & \\ 10 & 11 & 12 & 13 & 14 & 15 & & 16 & \end{pmatrix}, \quad (45)$$

and the corresponding periodic sequence [cf. (27) and (44)] is

$$\wp(S_1 \cap TS_1)=(1_3^s,1_4^u,2_1,1_5^u,2_2,1_6^s,2_3,(1_7)^c,2_3,1_8^u,2_2,$$
$$2_4,(1_1^s)^{\mathrm{cpo}},2_4,2_1,(1_2^s)^{\mathrm{prm}}), \quad (46)$$

where the period-2_4 orbit is new. The winding number sequence is

$$(1/1_3^s,1/1_4^u,2/3_1,1/2_5,2/4_2,1/2_6,2/4_3,(1/2_7)^c,2/4_3,1/2_8,$$
$$2/4_2,2/3_4,(1/1_1^s)^{\mathrm{cpo}},2/3_4,2/3_1,(1/1_2^s)^{\mathrm{prm}}). \quad (47)$$

The first pruning group is $(1/1_3,1/1_4)$. For the second group, except for the new period-$2/3_4$ po, the rest of the pruning sequence for (47) follows (43) with the right tangency, so that the following two pruning patterns are possible for the winding numbers 2/3 orbits (see Fig. 10):

(1) Type I bifurcations

$$
\begin{array}{c}
(2/3_1,1/2^u_5,2/4_2,1/2^s_6,\underline{2/4}_3,(1/2^s_7)^c,\underline{2/4}_3,1/2^u_8,2/4_2,2/3_4,(1/1^s_1)^{\mathrm{cpo}},2/3_4,2/3_1,(1/1^s_2)^{\mathrm{prm}})\\
\downarrow\\
(2/3_1,1/2^u_5,2/4_2,1/2^s_6,((\underline{1/2}^s_7)^c,\underline{1/2}^u_8),2/4_2,2/3_4,(1/1^s_1)^{\mathrm{cpo}},2/3_4,2/3_1,(1/1^s_2)^{\mathrm{prm}})\\
\downarrow\\
(2/3_1,1/2^u_5,\underline{2/4}_2,1/2^s_6,\underline{2/4}_2,2/3_4,(1/1^s_1)^{\mathrm{cpo}},2/3_4,2/3_1,(1/1^s_2)^{\mathrm{prm}})\\
\downarrow\\
(2/3_1,(\underline{1/2}^u_5,\underline{1/2}^s_6),2/3_4,(1/1^s_1)^{\mathrm{cpo}},2/3_4,2/3_1,(1/1^s_2)^{\mathrm{prm}})\\
\downarrow\\
(2/3_1,\underline{2/3}_4,(1/1^s_1)^{\mathrm{cpo}},\underline{2/3}_4,2/3_1,(1/1^s_2)^{\mathrm{prm}})\\
\downarrow\\
(\underline{2/3}_1,(1/1^s_1)^{\mathrm{cpo}},\underline{2/3}_1,(1/1^s_2)^{\mathrm{prm}})\\
\downarrow\\
((1/1^s_1)^{\mathrm{cpo}},(1/1^s_2)^{\mathrm{prm}}).
\end{array}
\tag{48}
$$

(2) Type *II* (tangent) bifurcation

$$
\begin{array}{c}
(2/3_1,1/2^u_5,2/4_2,1/2^s_6,\underline{2/4}_3,(1/2^s_7)^c,\underline{2/4}_3,1/2^u_8,2/4_2,2/3_4,(1/1^s_1)^{\mathrm{cpo}},2/3_4,2/3_1,(1/1_2)^{\mathrm{prm}})\\
\downarrow\\
(2/3_1,1/2^u_5,2/4_2,1/2^s_6,((\underline{1/2}^s_7)^c,\underline{1/2}^u_8),2/4_2,2/3_4,(1/1^s_1)^{\mathrm{cpo}},2/3_4,2/3_1,(1/1_2)^{\mathrm{prm}})\\
\downarrow\\
(2/3_1,1/2^u_5,\underline{2/4}_2,1/2^s_6,\underline{2/4}_2,2/3_4,(1/1^s_1)^{\mathrm{cpo}},2/3_4,2/3_1,(1/1_2)^{\mathrm{prm}})\\
\downarrow\\
(2/3_1,(\underline{1/2}^u_5,\underline{1/2}^s_6),2/3_4,(1/1^s_1)^{\mathrm{cpo}},2/3_4,2/3_1,(1/1_2)^{\mathrm{prm}})\\
\downarrow\\
((\underline{2/3}_1,\underline{2/3}_4),(1/1^s_1)^{\mathrm{cpo}},(\underline{2/3}_4,\underline{2/3}_1),(1/1_2)^{\mathrm{prm}})\\
\downarrow\\
((1/1^s_1)^{\mathrm{cpo}},(1/1^s_2)^{\mathrm{prm}}).
\end{array}
\tag{49}
$$

Pruning degeneracy occurs for pruning pattern (48) between $(2/4_3,(1/2)^c,2/4_3)$ and $(2/3_4,(1/1)^{\mathrm{cpo}},2/3_4)$; that is, we cannot determine the order of pruning of the $2/3_4$ and $2/4_3$ orbits. However, in order to have a pair of tangent bifurcations (2/3,2/3) in the pruning sequence, there can be no pruning degeneracy in (49) between $(2/4_3,(1/2)^c,2/4_3)$ and $(2/3_4,(1/1)^{\mathrm{cpo}},2/3_4)$. As β_{12} increases at fixed energy, we expect the pruning sequence of type *I* to occur first, followed by the type *II* sequence. Numerically, the pruning sequence (48) occurs for $\beta_{12}=0.02$, while the sequence (49) occurs at $\beta_{12}=0.022$. (The transition between the two types of behavior occurs at $\beta_{12}=0.2118$, cf. Fig. 11.)

4. Analysis of codimension-2 collisions for higher-order pos

The above pruning degeneracy between type *I* and *II* prunings for period-2 pos can be seen easily by considering the permutational representation for the po configuration $(2_i,2_j,1^{\mathrm{cpo}},2_j,2_i)$ (see Fig. 12):

$$
P(S_i\cap TS_i)=\begin{pmatrix}5&4&3&2&1\\1&2&3&4&5\end{pmatrix}. \tag{50}
$$

The permutation (50) is consistent not only with the occurrence of resonant period-2 bifurcations $(2_j,1^{\mathrm{cpo}},2_j)$ and $(2_i,1^{\mathrm{cpo}},2_i)$, but also with the tangent bifurcation $(2_i,2_j)$ and $(2_j,2_i)$ (cf. Sec. V). In (50), the pairs of columns $\left(\begin{smallmatrix}5&4\\1&2\end{smallmatrix}\right)$ and $\left(\begin{smallmatrix}2&1\\4&5\end{smallmatrix}\right)$, which are equivalent to po sequences $(2_i,2_j)$ and $(2_j,2_i)$, define the pruning sequence for the tangent bifurcation. The local behavior of the first iterate of S_1 is shown in Fig. 12, where the pruning degeneracy is apparent. For pruning of period-2 pos by tangent bifurcation, the two pairs of pos $(2_i,2_j)$ and $(2_j,2_i)$ must be pruned at the same energy E (fixed β_{12}). For period-3 pos, $(3_i,3_j,1,3_k,3_l)$, for which $P(S_i\cap T^3S_i)=\left(\begin{smallmatrix}1&2&3&4&5\\1&2&3&4&5\end{smallmatrix}\right)$, the two pairs of period-3 pos $(3_i,3_j)$ and $(3_k,3_l)$ are in general pruned at different E.

The pruning sequences ''before'' (48) and ''after'' (49) reveal the mechanism for tangency of the period-2 orbits. For small β_{12}, the two period-2 orbits, $2/3_1$ and $2/3_4$, are both pruned by type *I* bifurcations. As β_{12} increases, the two pos collide and separate to form a pair of pos pruned by type *II* (tangent) bifurcations (see Fig. 11). The collision of the two period-2 pos is an unlikely event requiring both energy E and coupling parameter β_{12} to have particular values; that is, the collision is a codimension-2 bifurcation. Such a codimension-2 bifurcation provides a generic mechanism for emergence of tangent bifurcations for period-n ($n\geqslant 2$) pos. Detailed examination of po behavior just before collision reveals a more complicated pruning and bifurcation scenario involving, for period-n ($n\neq 3$), an inverse pitchfork type bifurcation on the cpo, while for $n=3m$, an inverse tangent bifurcation occurs (see Fig. 13). The above pruning analysis shows two limiting regimes (type *I* and type *II*) for codimension-2 prunings/bifurcations as the coupling param-

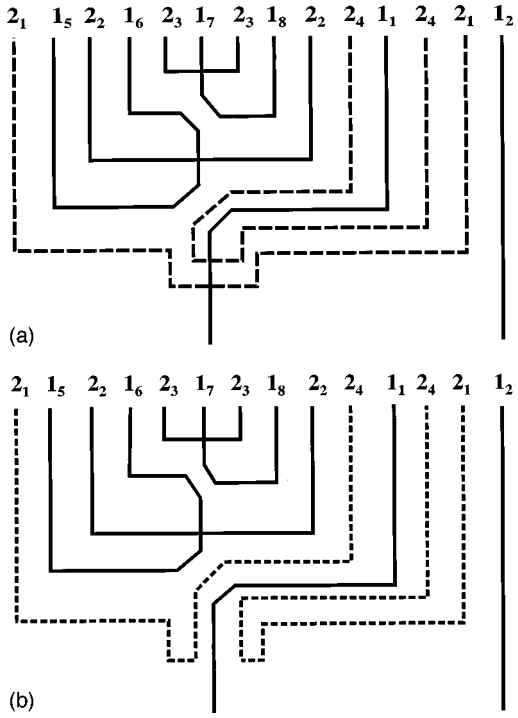

FIG. 10. Schematic bifurcation analysis for $S_1 \cap TS_1$. The relative ordering of period-1 and period-2 pos on the symmetry line S_1 is shown as a function of energy for fixed parameters $\beta_{11}=0.01$ and β_{12}, with β_{12} values larger than those of Fig. 8. Both sequences shown are found numerically. (a) $\beta_{12}=0.02$. For this case, the period-2 pos 2_1 and 2_4 are created by island-chain (type *I*) bifurcations [cf. Eq. (48)]. (b) $\beta_{12}=0.022$. For this case, the period-2 pos 2_4 and 2_1 are created by tangent bifurcation [type *II*, cf. Eq. (49)].

eter β_{12} is varied; application of local analysis such as normal form theory[30,32] can presumably describe the full details of the collision scenario. The pruning patterns discussed in Sec. V should therefore be taken to describe the net effect of more complicated prunings/bifurcation sequences (Fig. 14).

5. A possible mechanism for correlation between type II bifurcations

The number of intersections for $S_1 \cap T^2 S_1$ for $\beta_{12}=0.02$ and $E=6.98$ increases from 26 [see (29)] to 36, where a period-2_4 (two unit columns), and four period-4_{7-10} (four pairs of columns) pos are newly created. The permutational representation is

$$P(S_1 \cap T^2 S_1) = \begin{pmatrix} 1 & 36 & 3 & 34 & 9 & 26 & 27 & 8 & 5 & 32 & 11 \\ 1 & 2 & 3 & 4 & 5 & 6 & 7 & 8 & 9 & 10 & 11 \\ 24 & 13 & 22 & 15 & 20 & 17 & 18 & 19 & 16 & 21 & \\ 12 & 13 & 14 & 15 & 16 & 17 & 18 & 19 & 20 & 21 & \\ 14 & 23 & 12 & 31 & 6 & 7 & 28 & 29 & 30 & 25 & \\ 22 & 23 & 24 & 25 & 26 & 27 & 28 & 29 & 30 & 31 & \\ 10 & 33 & 4 & 35 & 2 & & & & & & \\ 32 & 33 & 34 & 35 & 36 & & & & & & \end{pmatrix}, \quad (51)$$

and the corresponding period sequence [cf. (30)], where the sequence (46) appears in the unit columns, is

$$\wp(P(S_1 \cap T^2 S_1)) = (1_3^s, 4_1, 1_4^u, 4_2, 4_7, 4_8, 4_9, 2_1, 4_7, 4_3, 1_5^u, 4_4, 2_2, 4_5, 1_6^s, 4_6, 2_3, (1_7^s)^c, 2_3, 4_6, 1_8^u, 4_5, 2_2, 4_4, 4_{10}, 4_8, 4_9, 2_4, (1_1^s)^{\mathrm{cpo}}, 2_4, 4_{10}, 4_3, 2_1, 4_2, (1_2^s)^{\mathrm{prm}}, 4_1). \quad (52)$$

The winding number sequence [cf. (31)] is

$$((1/1_3^s)^{\mathrm{spc}}, 3/3_1, 1/1_4^u, 4/5_2, 4/6_7, 4/6_8, 4/6_9, 2/3_1, 4/6_7, 4/7_3, 1/2_5^u, 4/8_4, 2/4_2, 4/8_5, 1/2_6^s, 4/8_6, 2/4_3, (1/2_7^s)^c, 2/4_3, 4/8_6, 1/2_8^u, 4/8_5, 2/4_2, 4/8_4, 4/7_{10}, 4/6_8, 4/6_9, 2/3_4, (1/1_1^s)^{\mathrm{cpo}}, 2/3_4, 4/7_{10}, 4/7_3, 2/3_1, 4/5_2, (1/1_2^s)^{\mathrm{prm}}, 3/3_1). \quad (53)$$

The pruning sequence in the first group is

$$(\underline{3/3_1}, (1/1_3^s)^{\mathrm{spc}}, \underline{3/3_1}, 1/1_4^u) \rightarrow ((\underline{1/1_3^s})^{\mathrm{spc}}, \underline{1/1_4^u}) \rightarrow (\varnothing), \quad (54)$$

where the $3/3_1$ po on the far right end of (53) now appears on the left. Note that the winding number for the period-4_1 po is $3/3_1$ rather than $4/3_1$. The pair $((1/1_3)^{\mathrm{spc}}, 1/1_4)$ is created (pruned) by a tangent bifurcation (type *II*); neither of these pos bifurcates from the cpo or the prm (see Sec. IV B). No third group bifurcation appears. The presence of the period sequence (46) in (53) provides a foundation for understanding the bifurcation tree for the period-4 orbits. In the second group, there are two pruning subgroups at $(1/2_7)^c$ and $(1/1_1)^{\mathrm{cpo}}$, respectively. Expanding the sequences (48) and (49) we have the two bifurcation sequences shown in Fig. 15. Both sequences shown are found numerically at $\beta_{12}=0.02$ and $\beta_{12}=0.022$, respectively.

For $\beta_{12}=0.02$ (cf. Fig. 15), the tangent bifurcation $((1/2_7)^c, 1/2_8)$ occurs, rather than $(1/2_6, (1/2_7)^c)$ [cf. (42) and (43)]. The presence of the po $(4/6_7)$ in (53) implies that the pair of pos $(4/6_8, 4/6_9)$ has to be involved in a tangent bifurcation. The pair therefore undergoes type *II* pruning. *The pruning of the pair of pos* $(4/6_8, 4/6_9)$ *provides a second example of the way in which the structure of the periodic sequence determines possible pruning of pos.* Note also that the corresponding columns in (51) for the pair are $\binom{26\ 27}{6\ 7}$ and $\binom{6\ 7}{26\ 27}$ (cf. the pruning pattern for type *II* in Sec. V). *When* the pair is pruned, however, cannot be predicted due to pruning degeneracy between $(4/6_8, 4/6_9)$ and the prunings at the center $(1/2_7)^c$. At $\beta_{12}=0.02$, it is found numerically that the pair is pruned right after the period-2 po $2/4_2$ is pruned. Following the final pruning by a pair of tangent bifurcations there are two possible routes, labeled (a) and (b):

(a) For (48), the period-$2/3_4$ po undergoes type *I* pruning, followed by two possible prunings (type *I* and *II*) for the orbits $(4/7_3, 4/7_{10})$. For the type *II* ($\beta_{12}=0.02$) case, there is pruning degeneracy between the resonant-2 bifurcation $(2/3_4, (1/1_1)^{\mathrm{cpo}}, 2/3_4)$ and tangent bifurcation $(4/7_3, 4/7_{10})$. Numerically, it is found that the tangent bifurcation $(4/7_3, 4/7_{10})$ occurs first, then $(2/3_4, (1/1_1)^{\mathrm{cpo}}, 2/3_4)$:

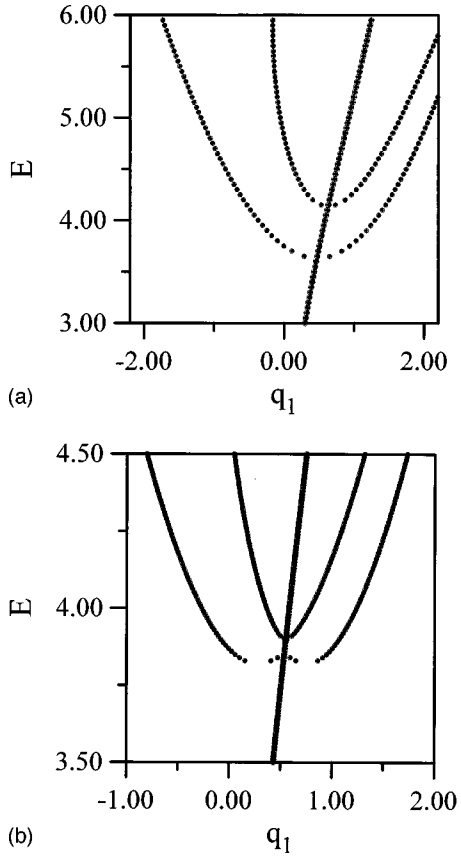

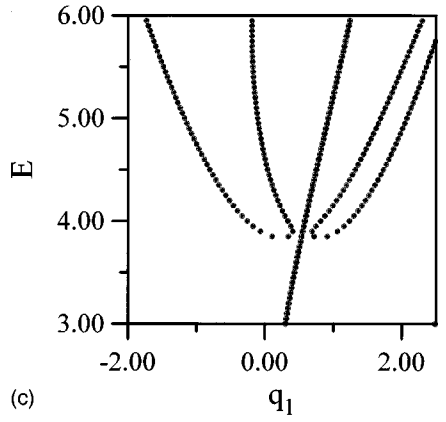

FIG. 11. Origin of tangent bifurcations via collisions of period-2 pos. (a) $\beta_{12}=0.021$. Here, both period-2 pos are created by type-*I* island-chain bifurcations [cf. Fig. 10(a)]. (b) $\beta_{12}=0.02117$. (c) $\beta_{12}=0.02118$. Here, period-2 pos are created by type-*II* tangent bifurcations [cf. Fig. 10(a)].

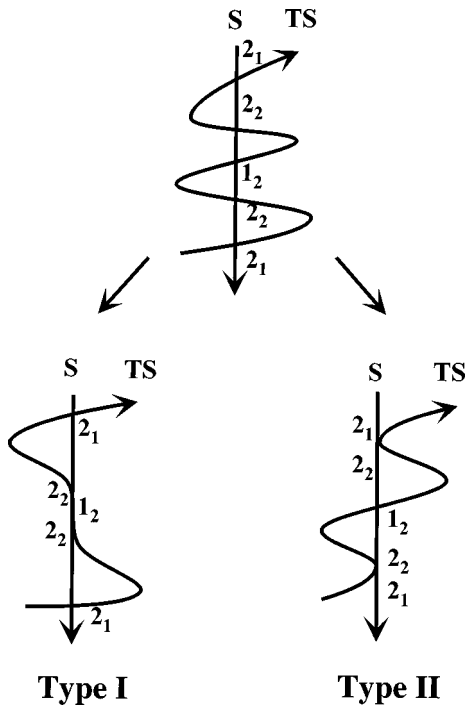

FIG. 12. Permutational representation and the local behavior of the first iterate of S_1, showing pruning degeneracy for the pruning of period-2 pos. The two limiting regimes for codimension-2 bifurcation/pruning are shown. The first case (type *I*) corresponds to island-chain bifurcations; the second (type-*II*) to creation of period-2 pos by tangent bifurcations.

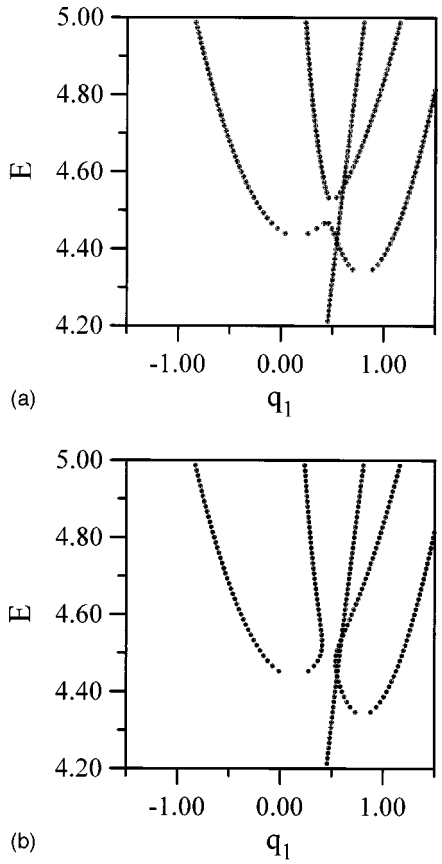

FIG. 13. Origin of tangent bifurcations via collisions of period-3 pos (sequential touch-and-go bifurcations). (a) $\beta_{12}=0.009810$. For this parameter value, each stable-unstable pair of period-3 pos is involved in a separate touch-and-go bifurcation. (b) $\beta_{12}=0.009818$. For this parameter value, one pair of period-3 pos is not involved in a touch-and-go bifurcation; the unstable po of the other pair is involved in two sequential touch-and-go bifurcations.

$$
\begin{array}{c}
(4/5_2,4/6_7,2/3_1,4/6_7,4/7_3,4/7_{10},\underline{2/3_4},(1/1_1^s)^{\mathrm{cpo}},\underline{2/3_4},4/7_{10},4/7_3,2/3_1,4/5_2,(1/1_2^s)^{\mathrm{prm}}) \\
\downarrow \\
I\left\{\begin{array}{c}
(4/5_2,4/6_7,2/3_1,4/6_7,4/7_3,\underline{4/7_{10}},(1/1_1^s)^{\mathrm{cpo}},\underline{4/7_{10}},4/7_3,2/3_1,4/5_2,(1/1_2^s)^{\mathrm{prm}}) \\
\downarrow \\
(4/5_2,4/6_7,2/3_1,4/6_7,\underline{4/7_3},(1/1_1^s)^{\mathrm{cpo}},\underline{4/7_3},2/3_1,4/5_2,(1/1_2^s)^{\mathrm{prm}})
\end{array}\right\} \\
\mathrm{or} \\
II\left\{\begin{array}{c}
(4/5_2,4/6_7,2/3_1,4/6_7,(\underline{4/7_3},\underline{4/7_{10}}),(2/3_4,(1/1_1^s)^{\mathrm{cpo}},2/3_4),(\underline{4/7_{10}},\underline{4/7_3}),2/3_1,4/5_2,(1/1_2^s)^{\mathrm{prm}}) \\
\downarrow \\
(4/5_2,4/6_7,2/3_1,4/6_7,\underline{2/3_4},(1/1_1^s)^{\mathrm{cpo}},\underline{2/3_4},2/3_1,4/5_2,(1/1_2^s)^{\mathrm{prm}})
\end{array}\right\} \\
\downarrow \\
(4/5_2,\underline{4/6_7^s},2/3_1^s,\underline{4/6_7^s},(1/1_1^s)^{\mathrm{cpo}},2/3_1,4/5_2,(1/1_2^s)^{\mathrm{prm}}) \\
\downarrow \\
(4/5_2,\underline{2/3_1^s},(1/1_1^s)^{\mathrm{cpo}},\underline{2/3_1^s},4/5_2,(1/1_2^s)^{\mathrm{prm}}) \\
\downarrow \\
(\underline{4/5_2},(1/1_1^s)^{\mathrm{cpo}},\underline{4/5_2},(1/1_2^s)^{\mathrm{prm}}) \\
\downarrow \\
((1/1_1^s)^{\mathrm{cpo}},(1/1_2^s)^{\mathrm{prm}}).
\end{array}
\tag{55}
$$

(b) For (49) (occurring at $\beta_{12}=0.022$), in order that the period-$2/3_4$ po be pruned as type *II*, the orbits $(4/7_3,4/7_{10})$ must be pruned as type *II*. In other words, if the period-4 po $4/7_{3\ \mathrm{or}\ 10}$ po undergoes type *I* bifurcation (the route a,I), so must the period-2 $2/3_{1\ \mathrm{or}\ 4}$ po:

$$
\begin{array}{c}
(4/5_2,4/6_7,2/3_1,4/6_7,(\underline{4/7_3},\underline{4/7_{10}}),2/3_4,(1/1_1^s)^{\mathrm{cpo}},2/3_4,(\underline{4/7_{10}},\underline{4/7_3}),2/3_1,4/5_2,(1/1_2^s)^{\mathrm{prm}}) \\
\downarrow \\
(4/5_2,\underline{4/6_7^s},2/3_1^s,\underline{4/6_7^s},2/3_4,(1/1_1^s)^{\mathrm{cpo}},2/3_4,2/3_1,4/5_2,(1/1_2^s)^{\mathrm{prm}}) \\
\downarrow \\
(4/5_2,(\underline{2/3_1^s},\underline{2/3_4^u}),(1/1_1^s)^{\mathrm{cpo}},(\underline{2/3_4^s},\underline{2/3_1^u}),4/5_2,(1/1_2^s)^{\mathrm{prm}}) \\
\downarrow \\
(\underline{4/5_2},(1/1_1^s)^{\mathrm{cpo}},\underline{4/5_2},(1/1_2^s)^{\mathrm{prm}}) \\
\downarrow \\
((1/1_1^s)^{\mathrm{cpo}},(1/1_2^s)^{\mathrm{prm}}).
\end{array}
\tag{56}
$$

The po $4/6_7$ bifurcates from the period-2 po $2/3_1$, which is therefore stable; the po $2/3_4$ is therefore unstable. Combining results of po pruning on S_1 with an analysis of po pruning on the S_2 symmetry line, the stabilities of more pos can be determined (e.g., the po $4/6_7$ is stable, cf. next section).

Numerically, type *I* bifurcation (the route a,I) does not occur since the period-2 po $2/3_4$ is not created yet at the value of β_{12} at which the period-4 po $4/7_{10}$ orbit appears by type *I* bifurcation; when the period-2 po $2/3_4$ is created by a resonant period-2 bifurcation, the route (a,II) occurs. Our analysis however clearly shows the possibility of correlation between bifurcations of orbits of different periods. Such correlations are expected for larger β_{12} and higher energy, since more newly created pos will appear in the sequence (53), and become involved in tangent bifurcations as the coupling constant β_{12} continues to increase.

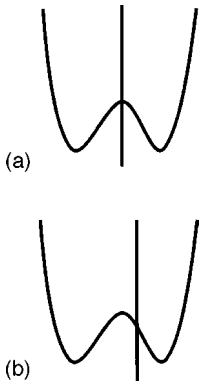

FIG. 14. (a) A complicated bifurcation scheme whose net effect is equivalent to a type *I* pruning. (b) Bifurcation scheme involving touch-and-go bifurcation whose net effect is equivalent to type *I* pruning.

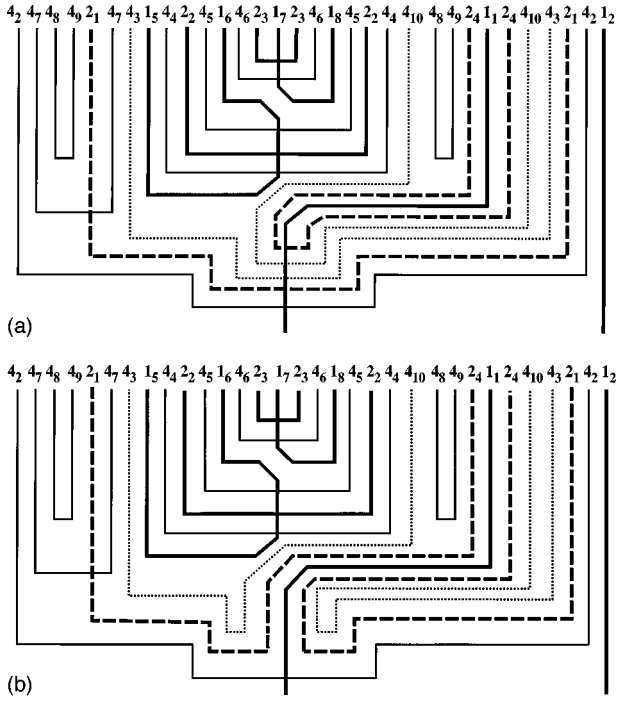

FIG. 15. Schematic bifurcation analysis for $S_1 \cap T^2 S_1$. The relative ordering of period-1, period-2 and period-4 pos on the symmetry line S_1 is shown as a function of energy for fixed parameters $\beta_{11}=0.01$ and β_{12}. Both sequences shown are found numerically. (a) Bifurcation diagram for the route (a,I) [see Eq. (55)]. (b) Bifurcation diagram for the route (b) [occurs numerically at $\beta_{12}=0.022$, see Eq. (56)].

Finally, from the pruning schemes shown above (55) and (56), the mechanism of onset of tangency for period-4 pos is seen to be the same as that of period-2 pos, namely, collision of period-4 bifurcations.

VII. BIFURCATION ANALYSIS ON S_2: PAIRING OF STABLE AND UNSTABLE PERIODIC ORBITS ON SYMMETRY LINES

So far, we have focused on the analysis of pos on the S_1 symmetry line. In this section we show how stability of pos on the two (S_1 and S_2) symmetry lines on Σ_1 can be found by analyzing pruning sequences on S_2. For $E=6.98$ and $\beta_{12}=0.02$, there are 16 and 32 intersections for $S_2 \cap TS_2$ and $S_2 \cap T^2 S_2$. Figure 2 shows that S_2 passes through the same period-1 pos as S_1 (see Appendix), but the relative positions of the cpo and the period-1 po $1/1_5$ are exchanged. This change of relative position is due to the fact that the symmetry line S_2 is not simply a straight line on Σ_1, but a more complicated curve (see Sec. II B). The permutational representation for $S_2 \cap TS_2$ is

$$P(S_2 \cap TS_2)=\begin{pmatrix} 1 & 2 & 15 & 6 & 5 & 6 & 13 & 8 & 11 \\ 1 & 2 & 3 & 4 & 5 & 4 & 7 & 8 & 9 \\ 10 & 9 & 12 & 7 & 14 & 3 & 16 \\ 10 & 11 & 12 & 13 & 14 & 15 & 16 \end{pmatrix}. \quad (57)$$

The period and winding number sequences [cf. (44) for po stabilities] are, respectively,

$$\wp(P(S_2 \cap TS_2))=((1_3^s)^{\mathrm{spc}},1_4^u,2_5,2_6,(1_1^s)^{\mathrm{cpo}},2_6,2_7, 1_6^s,2_8,1_7^c,2_8,1_8^u,2_7,1_5^u,2_5,(1_2^s)^{\mathrm{prm}}), \quad (58)$$

and

$$((1/1_3^s)^{\mathrm{spc}},1/1_4^u,2/3_5,2/3_6,(1/1_1^s)^{\mathrm{cpo}},2/3_6,2/4_7,1/2_6^s,2/4_8, (1/2_7^s)^c,2/4_8,1/2_8^u,2/4_7,1/2_5^u,2/3_5,(1/1_2^s)^{\mathrm{prm}}). \quad (59)$$

The first group is the tangent bifurcation of the spc and unstable resonant modes $((1/1)^{\mathrm{spc}},(1/1)^u)$. In the pruning sequence for the second group [cf. (48) and (49)], the period-2_5 and 2_6 pos are pruned as either type I or type II as follows:

$$\begin{array}{c} (2/3_5,(2/3_6,(1/1_1^s)^{\mathrm{cpo}},2/3_6),2/4_7,1/2_6^s,\underline{2/4_8},(1/2_7^s)^c,\underline{2/4_8},1/2_8^u,2/4_7,1/2_5^u,2/3_5,(1/1_2^s)^{\mathrm{prm}}) \\ \downarrow \\ (2/3_5,(2/3_6,(1/1_1^s)^{\mathrm{cpo}},2/3_6),2/4_7,1/2_6^s,((\underline{1/2_7^s})^c,\underline{1/2_8^u}),2/4_7,1/2_5^u,2/3_5,(1/1_2^s)^{\mathrm{prm}}) \\ \downarrow \\ (2/3_5,(2/3_6,(1/1_1^s)^{\mathrm{cpo}},2/3_6),\underline{2/4_7},1/2_6^s,\underline{2/4_7},1/2_5^u,2/3_5,(1/1_2^s)^{\mathrm{prm}}) \\ \downarrow \\ (2/3_5,(2/3_6,(1/1_1^s)^{\mathrm{cpo}},2/3_6),(\underline{1/2_6^s},\underline{1/2_5^u}),2/3_5,(1/1_2^s)^{\mathrm{prm}}) \\ \downarrow \\ I\left\{\begin{array}{c}(2/3_5,\underline{2/3_6},(1/1_1^s)^{\mathrm{cpo}},\underline{2/3_6},2/3_5,(1/1_2^s)^{\mathrm{prm}}) \\ \downarrow \\ (\underline{2/3_5},(1/1_1^s)^{\mathrm{cpo}},\underline{2/3_5},(1/1_2^s)^{\mathrm{prm}})\end{array}\right\} \\ \mathrm{or} \\ II((\underline{2/3_5^u},\underline{2/3_6^s}),(1/1_1^s)^{\mathrm{cpo}},(\underline{2/3_6^u},\underline{2/3_5^s}),(1/1_2^s)^{\mathrm{prm}}) \\ \downarrow \\ ((1/1)^{\mathrm{cpo}},(1/1)^{\mathrm{prm}}), \end{array} \quad (60)$$

For the type I pruning of period-2 pos $2/3_6$, pruning degeneracy between $(2/3_6,(1/1_1^s)^{\mathrm{cpo}},2/3_6)$ and $(2/4_8,(1/2_7^s)^c,2/4_8)$ occurs. However, in order to have a pair of tangent bifurcations $(2/3_5,2/3_6)$ in the pruning sequence, there can be no pruning degeneracy between $(2/3_6,(1/1)^{\mathrm{cpo}},2/3_6)$ and $(2/4_8,(1/2)^c,2/4_8)$.

The pos $(2/3_1^s,2/3_5)$, $(2/3_4^u,2/3_6)$, $(2/4_2,2/4_7)$, and $(2/4_3,2/4_8)$ [cf. (48) and (49)] form stable/unstable (Poincaré–Birkhoff) pairs, so that the po $2/3_5$ is unstable $(2/3_5^u)$ and the po $2/3_6$ is stable $(2/3_6^s)$. These pairings are consistent with the results of the Appendix on period-2 pos. One can determine the stability of pos in the pairs $(2/4_2,2/4_7)$ and $(2/4_3,2/4_8)$ by analyzing possible po prunings for higher order iterations $(n>2)$ or higher energy $(E>6.98)$. For the second iteration, the permutational representation is

$$P(S_2\cap T^2S_2)=\begin{pmatrix}1&32&3&30&5&28&11&8&9&10&7&26\\1&2&3&4&5&6&7&8&9&10&11&12\\13&22&15&20&17&18&19&16&21&14&&\\13&14&15&16&17&18&19&20&21&22&&\\25&24&23&12&27&6&29&4&31&2&&\\23&24&25&26&27&28&29&30&31&32&&\end{pmatrix}. \tag{61}$$

The period of [cf. (58)] and winding number sequences, respectively, are

$$\begin{aligned}\wp(P(S_2\cap T^2S_2))=(&1_3^s,4_{11},1_4^u,4_{12},2_5,4_{13},4_{14},2_6,(1_1^s)^{\mathrm{cpo}},\\&2_6,4_{14},4_{15},2_7,4_{16},1_6^s,4_{17},2_8,(1_7^s)^c,\\&2_8,4_{17},1_8^u,4_{16},4_{18},2_7,4_{18},4_{15},1_5^u,4_{13},\\&2_5,4_{12},(1_2^s)^{\mathrm{prm}},4_{11}),\end{aligned} \tag{62}$$

and

$$\begin{aligned}(&1/1_3^s,3/3_{11},1/1_4^u,4/5_{12},2/3_5,4/7_{13},4/7_{14},2/3_6,(1/1_1^s)^{\mathrm{cpo}},\\&2/3_6,4/7_{14},4/8_{15},2/4_7,4/8_{16},1/2_6^s,4/8_{17},2/4_8,(1/2_7^s)^c,\\&2/4_8,4/8_{17},1/2_8^u,4/8_{16},4/8_{18},2/4_7,4/8_{18},4/8_{15},1/2_5^u,\\&4/7_{13},2/3_5,4/5_{12},(1/1_2)^{\mathrm{prm}},3/3_{11}).\end{aligned} \tag{63}$$

Observe that there is no 4/6 po complementary to the period-$4/6_7$ on S_1 in (63). The reason is as follows: in the sequence (53), the po $4/6_7$ bifurcates from the stable period-2 po $2/3_1^s$, so that no bifurcation can occur on the complementary unstable period-2 po $2/3_5^u$ on S_2. Therefore, if the period-4 po 4/6 existed on S_2, it could only have been created by tangent bifurcation. This is impossible, as there is no stable period-2 po $2/3_1$ on S_2 from which the complementary 4/6 po would have to have bifurcated. There is therefore only one possible scenario; that is, the po $4/6_7$ on S_1 is created by a *period-doubling* bifurcation. This conclusion is confirmed numerically (see Fig. 16). The po $4/6_7$ is therefore stable before bifurcation and unstable after. Finally, if $r=2s$ for a type I pruning, (r_i,s,r_j) $(r,s\in Q)$, then the bifurcation is period-doubling or resonant island-chain [see pos $2/4_2$ in (42) and $2/4_8$ in (60)]; otherwise the bifurcation pattern is island-chain, except for $r=3s$, touch-and-go in our system. Note that the po $4/8_{18}$ is created by a period-doubling bifurcation.

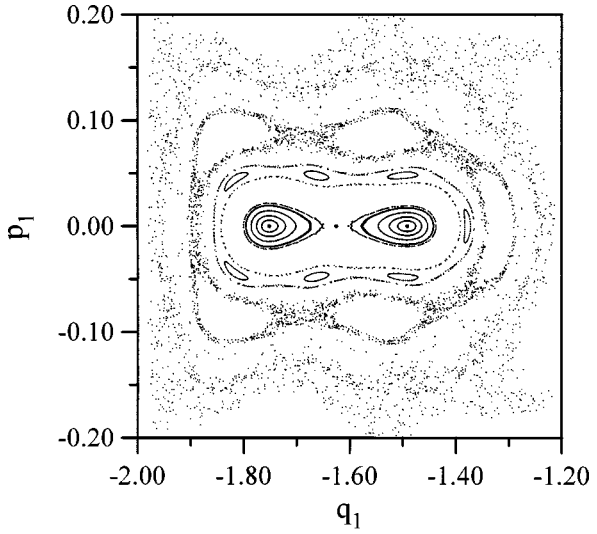

FIG. 16. Creation of a period-4 po on S_1 by period doubling. Analysis of stability of pos on the two symmetry lines S_1 and S_2 shows that the period-4 po $4/6_7$ on symmetry line S_1 must be created by a period-doubling bifurcation. This is confirmed numerically in the surface of section shown. Parameters are $E=5.68$, $\beta_{11}=0.01$, $\beta_{12}=0.02$.

We have analyzed pruning sequences for (63) before (type I) and after (type II) collision of the period-2 po pairs $(2/3_5,2/3_6)$ [cf. (60)].[37] Numerically observed bifurcation sequences corresponding to those of Fig. 15 are shown in Fig. 17.

Analysis of pruning reveals that the following correlation of bifurcations between the period-2 and the period-4 pos occurs: In order that the period-$2/3_6$ po be pruned as type II, the orbits $(4/7_{13},4/7_{14})$ must be pruned as type II (see Fig. 17). In other words, if the period-$4/7_{13\ \mathrm{or}\ 14}$ orbit undergoes type I bifurcation (a,I), so must the po $2/3_{5\ \mathrm{or}\ 6}$.

Comparing Figs. 15 and 17, the period-4 pos are found to be paired as $(4/5_2,4/5_{12})$, $(4/7_3,4/7_{13})$, $(4/7_{10},4/7_{14})$, $(4/8_4,4/8_{15})$, $(4/8_5,4/8_{16})$, and $(4/8_6,4/8_{17})$. The stability of those period-4 pos must be determined by examination of high-order iterates, especially the fourth order iterate.

VIII. CONCLUSION

In this paper we have studied classical periodic orbit (po) bifurcation sequences in a model molecular vibrational Hamiltonian consisting of two coupled Morse oscillators. The zeroth-order Hamiltonian has a single 1:1 resonance coupling term and is integrable; a second (2:1) coupling term of variable strength introduces nointegrability. Time reversal symmetry was exploited to systematically find (symmetric) pos by iteration of symmetry lines.

The permutational representation of Tsuchiya and Jaffé[28] was applied to analyze the intersection topology of a symmetry line with its iterates. Using the permutational representation, pruning rules describing possible local bifurcation be-

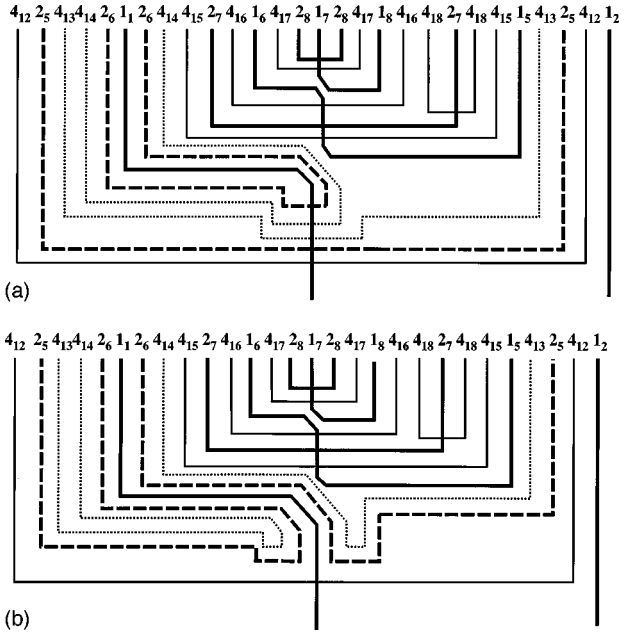

FIG. 17. Schematic bifurcation analysis for $S_2 \cap T^2 S_2$. The relative ordering of period-1, period-2 and period-4 pos on the symmetry line S_2 is shown as a function of energy for fixed parameters $\beta_{11}=0.01$ and β_{12}. Both sequences shown are found numerically. (a) Bifurcation diagram for the route in which period-2 pos undergo type-*I* bifurcations. ($\beta_{12}=0.02$). (b) Bifurcation diagram for the route in which period-2 pos undergo type-*II* bifurcations. (occurs numerically at $\beta_{12}=0.022$).

havior of pos were readily formulated. Moreover, a global understanding of allowed symmetric po bifurcation sequences together with po stabilities could be obtained.

Examination of classical (E,τ) plots for the coupled Morse system showed that breakdown of nonintegrable phase space structure is associated with the appearance of ubiquitous tangent (saddle-center) bifurcations. The mechanism for onset of tangent bifurcations was studied. For period-1 pos a ''disconnection'' mechanism applies (cf. Ref. 29). For period-2 and higher periods a different mechanism involving two parameter (codimension-2) collisions of bifurcations was found. Such collisions are accompanied by a breakdown of the zeroth-order winding numbers.

We have not investigated *nonsymmetric* pos in this paper. However, understanding bifurcations of symmetric pos can provide some information on nonsymmetric pos. Since all fundamental (period-one) pos exist on the symmetry lines, generic bifurcations of pos from fundamental pos occur on the symmetry lines. Tangent bifurcations, except for those on symmetry lines, will produce nonsymmetric pos. In the area-preserving Hénon map, tangent bifurcations on the symmetry lines have been shown to accumulate on (symmetric) homoclinic orbit bifurcations on symmetry lines.[28] In analogous fashion, a set of non-symmetric pos could be associated with nonsymmetric homoclinic orbit bifurcations.

The present work on the classical mechanics of the coupled Morse system forms the foundation for an analysis of the classical-quantum correspondence. This analysis will be presented elsewhere.[19] Our results point to the influence of non-symmetric pos on the quantum (E,τ) spectrum.[19]

With regard to the semiclassical mechanics of the system under study, it is interesting to speculate on possible semiclassical manifestations of the different possible bifurcation sequences. Different sequences might be characterized by different patterns of singularities, and so lead to qualitatively different deviations from GOE spectral statistics.[38]

Finally, we note that the pruning analysis using a permutational representation can also be applied to homoclinic orbits as well as pos.[28] Just as sequences of pos are known to converge to homoclinic orbits, so sequences of po tangent bifurcations can converge to homoclinic tangencies. Application of these ideas to the semiclassical mechanics of homoclinic tangles[39] would be of interest.

ACKNOWLEDGMENT

This research was supported by the National Science Foundation, under NSF Grant No. CHE-9709575.

APPENDIX

1. Period-1 and period-2 pos on symmetry lines S_1 and S_2

Let $\mathbf{z}\in S_1$ be a periodic point of period one, $T\mathbf{z}=\mathbf{z}$. Then $\mathbf{z}$ also lies on S_2, $\mathbf{z}\in S_2$:

$$T\mathbf{z}=I_2 I_1 \mathbf{z}=I_2\mathbf{z}=\mathbf{z}. \tag{A1}$$

Let $\mathbf{z}\in S_1$ be a periodic point of period two on S_1, $T^2\mathbf{z}=\mathbf{z}$. Then $\mathbf{z}$ does not lie on S_2, $\mathbf{z}\notin S_2$. This is proved by contradiction: noting that $T^{-1}=I_1 I_2$, and assuming $I_2\mathbf{z}=\mathbf{z}$, we have

$$\mathbf{z}=I_2\mathbf{z}=I_2 T^2\mathbf{z}=I_1 T\mathbf{z}=T^{-1}I_1\mathbf{z}=T^{-1}\mathbf{z}=T\mathbf{z}\equiv\mathbf{z}'. \tag{A2}$$

However, $\mathbf{z}\neq\mathbf{z}'$ by hypothesis, so we have a contradiction.

The same results clearly hold with S_1 and S_2 interchanged. Moreover, these results are true regardless of the nature of the dynamics (regular or chaotic).

2. Generating higher order permutations from $P(S_i \cap TS_i)$

Without loss of generality, one of the two involution operators I_i can be always taken to be a reflection. Because periodicities of symmetric pos cannot change unless the associated permutation changes, any intersection configuration, $S_i \cap T^n S_i$, can be deformed so that S_i becomes a straight line. Higher order iterates are generated from the given $P(S_i \cap TS_i)$ as follows. The inverse image of S_i is obtained by reflection along S_i, $I_i(TS_i)=T^{-1}S_i$, so that the intersection between $T^{-1}S_i$ and TS_i, i.e., the permutation $P(T^{-1}S_i \cap TS_i)$, is obtained uniquely. Invariance of the permutation (eq. 14) then determines $P(S_i \cap T^2 S_i)$:

$$P(T^{-1}S_i \cap TS_i)=P(S_i \cap T^2 S_i). \tag{A3}$$

Repeating the same procedure for $T^2 S_i$ and continuing for higher order iterates gives all permutations $P(S_i \cap T^{2^n} S_i)$, $(n\geqslant 0)$. It is important to note that the permutation for the (2^n)th iterate is uniquely determined from $P(S_i \cap TS_i)$ regardless of the nature of the dynamics (integrable, chaotic (mixed), or hyperbolic).

In mixed systems, difficulties occur in determining permutations $P(S_i \cap T^m S_i)$, m a prime number. Consider, for example, the permutation $P(S_i \cap T^3 S_i)$. From the above, we know $P(S_i \cap T^4 S_i)$, which is equivalent to $P(T^{-1} S_i \cap T^3 S_i)$. Then knowledge of the permutation $P(T^{-1} S_i \cap T^3 S_i)$ and the shape of $T^{-1} S_i$ determines the shape of $T^3 S_i$. Knowledge of the shape of the $T^3 S_i$ is not however sufficient to determine $P(S_i \cap T^3 S_i)$, due to its unknown position relative to the straight line S_i. Additional information is given by $P(T^{-1} S_i \cap T^2 S_i)$, where the shapes of $T^{-1} S_i$ and $T^2 S_i$ are known. The fact that the set of pos for $S_i \cap T^{-1} S_i$, which is equivalently to that of $S_i \cap T S_i$, is a subset of pos for $S_i \cap T^2 S_i$, gives information on the way in which $T^{-1} S_i$ and $T^2 S_i$, hence S_i and $T^3 S_i$, can intersect, but this is still in general not enough to determine $P(S_i \cap T^3 S_i)$.

These difficulties in generating higher order permutations have their origin in the fact that regular and chaotic components coexist in an extremely complicated manner in the phase space of mixed systems. By contrast, in the fully chaotic limit of the Hénon map, the number of intersections is maximal at each iteration, so that all permutations $P(S_i \cap T^\nu S_i)$ can be determined.[28]

[1] H. Poincaré, *New Methods of Celestial Mechanics* (AIP, New York, 1993).
[2] G. D. Birkhoff, *Dynamical Systems* (AMS, Providence, 1927).
[3] R. S. MacKay and J. D. Meiss, *Hamiltonian Dynamical Systems* (Hilger, Berlin, 1987).
[4] See, for example, P. Cvitanovic, Physica D **51**, 138 (1991); **83**, 109 (1995).
[5] K. R. Meyer, Trans. Am. Math. Soc. **149**, 95 (1970); K. R. Meyer and G. R. Hall, *Introduction to Dynamical Systems and the N-body Problem* (Springer, New York, 1992).
[6] M. C. Gutzwiller, *Chaos in Classical and Quantum Mechanics* (Springer Verlag, Berlin, 1990).
[7] M. S. Child, *Semiclassical Mechanics with Molecular Applications* (Oxford, New York, 1991); M. Brack and R. K. Bhaduri, *Semiclassical Physics* (Addison-Wesley, Reading, MA, 1997).
[8] H. Friedrich and D. Wintgen, Phys. Rep. **183**, 37 (1989).
[9] See, for example, G. Tanner, K. Richter, and J-M. Rost, Rev. Mod. Phys. (to appear), and references therein.
[10] See, for example, R. Schinke, *Photodissociation Dynamics* (Cambridge University Press, Cambridge, UK, 1993), Chap. 8.
[11] J. M. Mao and J. B. Delos, Phys. Rev. A **45**, 1746 (1992).
[12] H. S. Taylor, Acc. Chem. Res. **22**, 263 (1989); S. C. Farantos, Int. Rev. Phys. Chem. **15**, 345 (1996).
[13] G. S. Ezra, in *Advances in Classical Trajectory Methods, Vol. 3*, edited by W. L. Hase (JAI, New York, 1998).
[14] P. Gaspard and P. van Ede van der Pals, J. Chem. Phys. **110**, 5611 (1999).
[15] R. S. MacKay, J. D. Meiss, and I. C. Percival, Physica D **28**, 1 (1987).
[16] M. J. Davis, J. Chem. Phys. **107**, 4507 (1997).
[17] M. J. Davis, Int. Rev. Phys. Chem. **14**, 15 (1995).
[18] See, for example, R. Marquardt, M. Quack, J. Stohner, and E. Sutcliffe, J. Chem. Soc., Faraday Trans. 2 **86**, 1173 (1986).
[19] M. Tsuchiya and G. S. Ezra (work in progress).
[20] L. Xiao and M. E. Kellman, J. Chem. Phys. **90**, 6086 (1989); Z. Li, L. Xiao, and M. E. Kellman, *ibid.* **92**, 2251 (1990); L. Xiao and M. E. Kellman, *ibid.* **93**, 5805 (1990).
[21] L. Xiao and M. E. Kellman, J. Chem. Phys. **93**, 5821 (1990); J. Svitak, Z. Li, J. Rose, and M. E. Kellman, *ibid.* **102**, 4340 (1995).
[22] D. C. Rouben and G. S. Ezra, J. Chem. Phys. **103**, 1375 (1995); G. S. Ezra, *ibid.* **104**, 26 (1996).
[23] M. Joyeux, Chem. Phys. Lett. **247**, 454 (1995).
[24] A. J. Lichtenberg and M. A. Lieberman, *Regular and Stochastic Motion* (Springer, Berlin, 1983).
[25] R. DeVogelaere, in *Contributions to the Theory of Nonlinear Oscillations*, Vol. 4, edited by S. Lefschetz (Princeton University Press, NJ, 1958), p. 35.
[26] J. M. Greene, AIP Conf. Proc. **57**, 257 (1979).
[27] J. M. Greene, R. S. MacKay, F. Vivaldi, and M. J. Feigenbaum, Physica D **3**, 468 (1981).
[28] M. Tsuchiya, Ph.D. thesis, West Virginia University, 1995; M. Tsuchiya and C. Jaffé, preprint.
[29] T. Weston and M. S. Child, Chem. Phys. Lett. **262**, 751 (1996). See also S. Cho and M. S. Child, Mol. Phys. **81**, 447 (1994), Ref. 21.
[30] D. A. Sadovskii, J. A. Shaw, and J. B. Delos, Phys. Rev. Lett. **75**, 2120 (1995); D. A. Sadovskii and J. B. Delos, Phys. Rev. E **54**, 2033 (1996).
[31] K. R. Meyer, J. B. Delos, and J.-M. Mao, in *Conservative Systems and Quantum Chaos*, edited by L. M. Bates and D. L. Rod (American Mathematical Society, Providence, 1996).
[32] H. Schomerus, J. Phys. A **31**, 4167 (1998).
[33] G. H. Hardy and E. M. Wright, *An Introduction to the Theory of Numbers* (Oxford University Press, New York, 1979).
[34] J. Laskar, Physica D **67**, 257 (1993); J. Laskar, C. Froeschlé, and A. Celletti, *ibid.* **56**, 253 (1992).
[35] L. E. Fried and G. S. Ezra, J. Chem. Phys. **86**, 6270 (1987); M. E. Kellman, *ibid.* **93**, 6630 (1990).
[36] Such dynamically defined surfaces of section have been used previously by C. Jaffé (private communication).
[37] M. Tsuchiya and G. S. Ezra (unpublished).
[38] M. V. Berry, J. P. Keating, and S. D. Prado, J. Phys. A **31**, L245 (1998).
[39] S. Tomsovic and E. J. Heller, Phys. Rev. E **47**, 282 (1993).